Citation: Hirt C., M. Rexer, M. Scheinert, R. Pail, S. Claessens and S. Holmes (2015), A new degree-2190 (10 km resolution) gravity field model for Antarctica developed from GRACE, GOCE and Bedmap2 data. Journal of Geodesy 90(2), 105-127, doi: 10.1007/s00190-015-0857-6.

A new degree-2190 (10 km resolution) gravity field model for Antarctica developed from GRACE, GOCE and Bedmap2 data

Christian Hirt [1,2], Moritz Rexer [2], Mirko Scheinert [3], Roland Pail [2], Sten Claessens [1] , Simon Holmes [4]

[1] Western Australian Geodesy Group & the Institute for Geoscience Research & Department of Spatial Sciences, Curtin University, Perth, Australia

[2] Institute for Advanced Study & Institute for Astronomical and Physical Geodesy, Technische Universität München, Germany

[3] Institut für Planetare Geodäsie, Technische Universität Dresden, Germany

[4] SGT Inc., Greenbelt, USA, USA

Corresponding Author: Christian Hirt, Email: c.hirt@tum.de

Abstract

The current high-degree global geopotential models EGM2008 and EIGEN-6C4 resolve gravity field structures to ~10 km spatial scales over most parts of the of Earth's surface. However, a notable exception is continental Antarctica, where the gravity information in these and other recent models is based on satellite gravimetry observations only, and thus limited to about ~80-120 km spatial scales.

Here we present a new degree-2190 global gravity model (GGM) that for the first time improves the spatial resolution of the gravity field over the whole of continental Antarctica to ~10 km spatial scales. The new model called SatGravRET2014 is a combination of recent GRACE and GOCE satellite gravimetry with gravitational signals derived from the 2013 Bedmap2 topography/ice thickness/bedrock model with gravity forward modelling in ellipsoidal approximation. Bedmap2 is a significantly improved description of the topographic mass distribution over the Antarctic region based on a multitude of topographic surveys, and a well-suited source for modelling short-scale gravity signals as we show in our study. We describe the development of SatGravRET2014 which entirely relies on spherical harmonic modelling techniques. Details are provided on the least-squares combination procedures and on the conversion of topography to implied gravitational potential. The main outcome of our work is the SatGravRET2014 spherical harmonic series expansion to degree 2190, and derived high-resolution grids of 3D-synthesized gravity and quasigeoid effects over the whole of Antarctica.

For validation, six data sets from the IAG Subcommission 2.4f "Gravity and Geoid in Antarctica" (AntGG) database were used comprising a total of 1,092,981 airborne gravimetric observations. All subsets consistently show that the Bedmap2-based short-scale gravity modelling improves the agreement over satellite-only data considerably (improvement rates ranging between 9% and 75% with standard deviations from residuals between SatGravRET2014 and AntGG gravity ranging between 8 and 25 mGal). For comparison purposes, a degree-2190 GGM was generated based on the year-2001 Bedmap1 (using the ETOPO1 topography) instead of 2013 Bedmap2 topography product. Comparison of both GGMs against AntGG consistently reveals a closer fit over all test areas when Bedmap2 is used. This experiment provides evidence for clear improvements in Bedmap2 topographic information over

Bedmap1 at spatial scales of ~80-10 km, obtained from independent gravity data used as validation tool.

As a general conclusion, our modelling effort fills – in approximation – some gaps in short-scale gravity knowledge over Antarctica and demonstrates the value of the Bedmap2 topography data for short-scale gravity refinement in GGMs. SatGravRET2014 can be used, e.g., as a reference model for future gravity modelling efforts over Antarctica, e.g., as foundation for a combination with the AntGG data set to obtain further improved gravity information.

Keywords

GRACE, GOCE, Geopotential Model, Gravity, Topography, Bedmap2, Forward gravity modelling, Antarctica

1 Introduction

Accurate knowledge of the gravity field over Antarctica is required for several geoscience and environmental applications, as diverse as ice mass monitoring (Shepherd et al. 2012), topographic heighting with satellite systems, establishment and unification of underlying height reference systems (Rummel 2013), investigation and modelling of the crustal thickness (O'Donnell and Nyblade 2013, McKenzie et al. 2015), estimation of ice thicknesses through inversion (Fretwell et al. 2013) and investigation of geological signatures (von Frese et al. 2009, Studinger et al. 2004).

Because of the harsh conditions over most of Antarctica, the determination of the gravity field with terrestrial methods (ground gravimetric observations) is notoriously difficult (Scheinert 2012). Significant progress in gravity mapping has been made over the years with dedicated airborne gravimetric campaigns over selected regions (e.g., Forsberg et al. 2011; Scheinert 2012; Scheinert et al., 2015) and – at a continental scale – by the GRACE (Gravity Recovery and Climate Experiment), e.g., Mayer-Gürr et al. 2010, and GOCE (Gravity field and steady-state Ocean Circulation Explorer) satellite gravimetry missions (e.g., Rummel et al. 2011, van der Meijde et al. 2015).

Yet our knowledge of Antarctica's gravity field is far from being complete. Gravity maps from recent satellite gravimetry do not exceed a spatial resolution of about ~115-125 km (GRACE) and ~70-80 km (GOCE), e.g., Brockmann et al. (2014), Hirt et al. (2015). While airborne gravimetry is capable of extending the gravity mapping resolution to ~5-8 km (Forsberg et al. 2011), regions of significant extent are still devoid of airborne data. This includes the Southern Pole region (South of -83.3° latitude, also known as the "polar gap") that has not been directly observed due to GOCE's orbit inclination (van der Meijde et al. 2015). Gravity data compilations, notably those by the IAG Subcommission 2.4f "Gravity and Geoid in Antarctica" (AntGG) combine various airborne gravity surveys with the few available ground gravimetric observations (Scheinert et al. 2008; Scheinert 2012; Scheinert et al. 2015). Notwithstanding all these notable efforts, current Antarctic gravity maps are spectrally and spatially less complete than gravity maps/models over continents with good gravity data coverage such as Australia, Europe and North America.

The severities associated with high-resolution determination of Antarctica's gravity field are manifested in recent degree-2190 global geopotential models (GGMs) of Earth's static gravity field, too. Both in case of the EGM2008 model (Pavlis et al. 2012) that was released in 2008, and in the more recent EIGEN-6C4 (Förste et al. 2014), gravity information over continental Antarctica is from satellite gravimetry only. No attempt has been made in these models to enhance the resolution of the satellite-only gravity data over continental Antarctica (Pavlis et al. 2012.; C. Förste 2015, pers. comm.).

As topic of the present study we refine the gravity field over continental Antarctica for the first time to degree 2190 (about 10 km spatial resolution in latitude direction) through a combination of recent

GRACE and GOCE satellite gravimetry with gravity effects derived from detailed topographic mass modelling. Antarctica's topographic masses are now reasonably well known through the Bedmap2 data set (Fretwell et al. 2013). Bedmap2 is a concerted international effort of 35 scientific institutions providing high-resolution topography grids – encompassing topographic heights of ice-free land, ice sheet thickness, bedrock (i.e., sub-ice-topography) and bathymetric depths along the coasts – from a multitude of past and recent survey campaigns. Gravity derived from the Bedmap2 topographic masses was already found to offer high correlation with GOCE gravimetry (Hirt 2014), encouraging the use of the Bedmap2 product for gravity field refinement as done in this study.

This paper is organised as follows. Section 2 describes the data sets used in this study, including the GGMs from the GRACE and GOCE satellite missions, the Bedmap2 topography product, as incorporated in the Earth2014 global topography suite (Hirt and Rexer 2015), and observations from the AntGG gravity database which we use for validation purposes. For the forward modelling of gravity effects we apply the Claessens and Hirt (2013) computation approach which delivers the potential of the Bedmap2 topographic masses in spherical harmonics and in ellipsoidal approximation (i.e., masses are arranged at the surface of a mass-ellipsoid), which is compatible with most other GGMs (Section 3.1). For the combination of GRACE with GOCE and Bedmap2-implied gravity, a least-squares combination technique is applied at normal equation level, providing some remedy to the GOCE polar gap problem. This procedure yields a new spherical harmonic model complete to degree 2190 with the long to medium wavelengths defined through satellite data and short-wavelength information through Bedmap2 (Section 3.2). Gravity disturbances and quasigeoid undulations are obtained through three-dimensional spherical harmonic synthesis (at Antarctica's topographic surface) using the set of spherical harmonic coefficients of our combined GRACE/GOCE/Bedmap2 model (Section 3.3).

The main results of this work – the SatGravRET2014 spherical harmonic expansion and derived quasigeoid and gravity maps over continental Antarctica with 10 km spatial resolution – are presented and discussed in Section 4. Several modelling variants (using different weighting schemes for combining satellite with Bedmap2 data) are compared and validated using AntGG data sets showing the effectiveness of our gravity modelling (Section 5). We also include solutions using older Bedmap1 (Lythe et al. 2001) data showing the Bedmap2-added value for our gravity field solutions. This extends the Bedmap2 validation experiment presented in Hirt (2014) towards the short spatial scales. The results are discussed and conclusions are drawn along with suggestions for future work in Section 6.

There are many other methods that are capable of delivering detailed gravity field models. The remove-compute-restore (RCR) technique has been applied regionally by Schwabe et al. (2012) over the Antarctic Peninsula and in Schwabe et al. (2014) to derive a high-resolution geoid model over the Lake Vostok area, by Scheinert et al. (2008) over the Prince Charles Mountains and – offshore – over the Weddell Sea region by Schwabe and Scheinert (2014). In these studies, satellite and airborne gravity observations were refined with topographic information using the residual terrain modelling (RTM) technique (Forsberg 1984a). In contrast to these previous studies, we here tackle the whole of Antarctica, and work directly in spherical harmonics which is convenient in view of creating an improved GGM over Antarctica. Different to the previous works, ground-based and airborne gravity are not used as input data here; we deliberately use the AntGG gravity observations for validation only in order to benchmark the performance of the GOCE/GRACE/Bedmap2 solution. This is important for those parts of Antarctica which remain without ground-based/airborne gravity observations in the near future. In principle, AntGG (Scheinert et al., 2015) residual information can be added to the gravity field (not done here).

The gravity forward modelling method applied in this paper has been used successfully for computation of new band-limited GOCE Bouguer gravity maps over Antarctica (Hirt 2014), for

generation of a full-scale EGM2008 Bouguer global gravity map (Claessens and Hirt 2013) and for evaluation of recent geopotential models over Antarctica and elsewhere (Hirt et al. 2015). In the present study, the Claessens and Hirt (2013) forward modelling approach is used for a "direct fill-in" of topography-implied gravity at short spatial scales not resolved by GRACE/GOCE satellite gravimetry. This is a novel application. Our method is related to the RTM technique by Pavlis et al. (2007) used to fill-in gravity information derived from topography into EGM2008 over some parts of Earth (but not Antarctica). Both methods augment measured gravity with topography-implied gravity at short scales in the construction of spherical harmonic models. Different to Pavlis et al. (2007) we apply a spectral-domain forward modelling through expansion of the topographic potential into powers of the topography, focus on Antarctica, and model ice and water masses too from Bedmap2 which is the newest topography data compilation available.

2 Data

2.1 Satellite gravimetry

To describe the long- and medium-wavelength components of the Earth's static gravity field we use the ITG-Grace2010s (Mayer-Gürr et al. 2010) and the unconstrained GOCE-TIM5* (Brockmann et al. 2014) models. Both models represent the disturbing potential of the gravitational field via sets of spherical harmonic coefficients (SHCs). The ITG-Grace2010s model is a long-term mean gravity field based on seven years of GRACE mission data (K-band ranges and kinematic orbits) collected between August 2002 and August 2009. It offers a formal resolution to degree and order 180 while being highly accurate to harmonic degree ~150-160 (spatial scales of ~125 km).

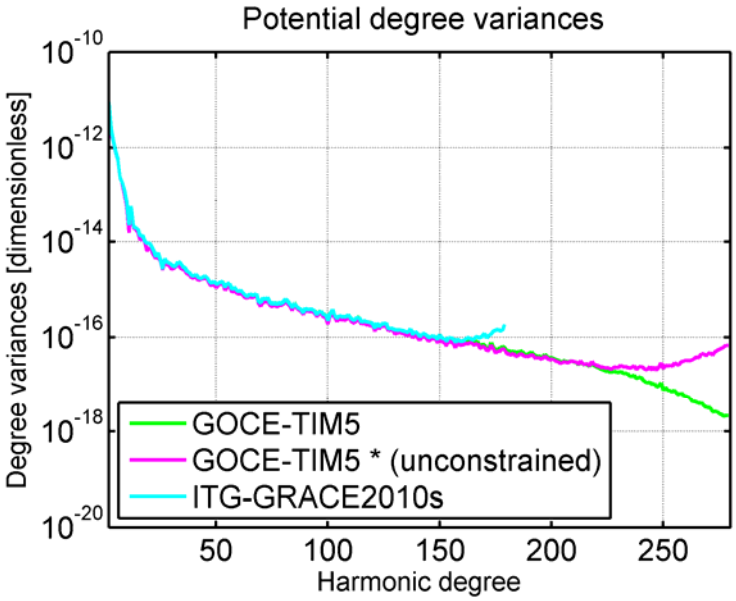

Fig. 1 Potential degree variances of GGMs from satellite gravimetry: ITG-Grace2010s (light blue), GOCE-TIM5* (magenta) and GOCE-TIM5 (green).

The GOCE-TIM5* model has been derived by the so-called time-wise approach (e.g., Pail et al. 2011) deploying ESA (European Space Agency)'s GOCE High-level Processing Facility. Different to the official GOCE-TIM5 release (available, e.g., at http://icgem.gfz-potsdam.de/ICGEM/) the GOCE-TIM5* model is an unconstrained solution, in that neither the Kaula rule-of-thumb has been applied to constrain the short-scale spectral behaviour of the model, nor the near-zonal spherical harmonic coefficients affected by the polar observation gap (due to GOCE satellite's orbital inclination) were regularized in any way. Like GOCE-TIM5, GOCE-TIM5* relies on a total of 42 months of data (satellite gravity gradiometry and GPS high-low satellite tracking) collected aboard the GOCE satellite between

November 2009 and October 2013 (Brockmann et al. 2014). It provides a formal gravity field resolution to degree and order 280 while effectively resolving the field to about degree ~240 equivalent to spatial scales of ~85 km (Brockmann et al. 2014, Hirt et al. 2015).

The dimensionless potential degree variances of ITG-Grace2010s and GOCE-TIM5* are shown together with those from the official GOCE-TIM5 solution in Fig. 1. Note that near-zonal coefficients were excluded in the computation of the GOCE-TIM5* degree variances, following the rule for polar gap-affected coefficients by Sneeuw and van Gelderen (1997) in order to reduce the impact of the GOCE polar observation gap on the GOCE-TIM5* spectrum. The affected coefficient groups will be later stabilized using GRACE and topographic information (Section 3.2). For both ITG-Grace2010s and GOCE-TIM5* full normal equations are used to model the stochastic properties of the spherical harmonic coefficients, facilitating the development of our combined gravity field model. The official GOCE-TIM5 model is used in Sections 4 and 5 in order to demonstrate the improvements conferred by our forward modelling over satellite-only gravity.

2.2 Topographic masses

In order to describe the topographic masses over continental Antarctica and surrounding waters we rely primarily on the Bedmap2 product (Fretwell et al. 2013) incorporated into the Earth2014 global topography model (Hirt and Rexer 2015). The distribution of Earth2014 data sources and land types is shown in Fig. 2 and selected layers of Earth2014 are shown in Fig. 3 over the Antarctic region.

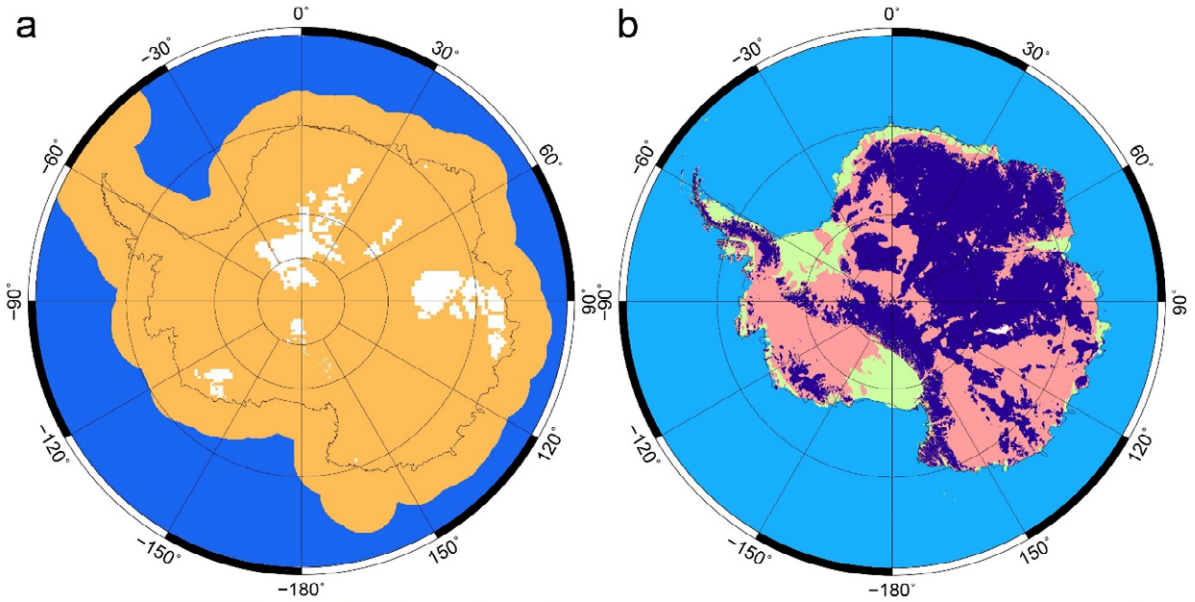

Fig. 2 Topography data used in this study. Panel a: Earth2014 data sources (Bedmap2 in orange and white, SRTM30_PLUS in blue) and areas without direct bedrock measurements (white). Panel b: Earth2014 land types over Antarctica (light blue – oceans, green – ice shelves, red – ice-free land, magenta - ice sheet with bedrock below mean sea level (MSL), dark blue – ice sheet with bedrock above MSL, white – Lake Vostok).

Bedmap2 describes ice-sheet and ice-shelf thickness, bedrock (the subglacial topography), bathymetry (sea floor topography) and land topography over ice-free land in terms of 1 km-resolution grids. The Bedmap2 topography grids are based on a variety of airborne and satellite observations, among them ice-penetrating airborne radar echo sounding (RES, for ice thickness), satellite radar altimetry (for surface elevations) and depth soundings (for bathymetry), cf. Fretwell et al. (2013). Bedmap2 incorporates results from many geophysical survey campaigns over Antarctica and provides considerably improved data (Fig 3a,b,c and Fig. 4) in comparison to its precursor Bedmap1 (Lythe et al. 2001). In Bedmap2, 36% of bedrock heights are based on direct measurements (mostly RES but also

seismics), compared to 17% in Bedmap1 (at 5 km resolution). Notwithstanding, there are still uncharted areas without direct bedrock observations (white areas in Fig. 2a) where Bedmap2 ice thickness and bedrock is based on an indirect estimation from inversion of GOCE satellite gravimetry (Fretwell et al. 2013). Over these areas, the bedrock information is not detailed and affected by uncertainties at the 1-km level (Fretwell et al. 2013).

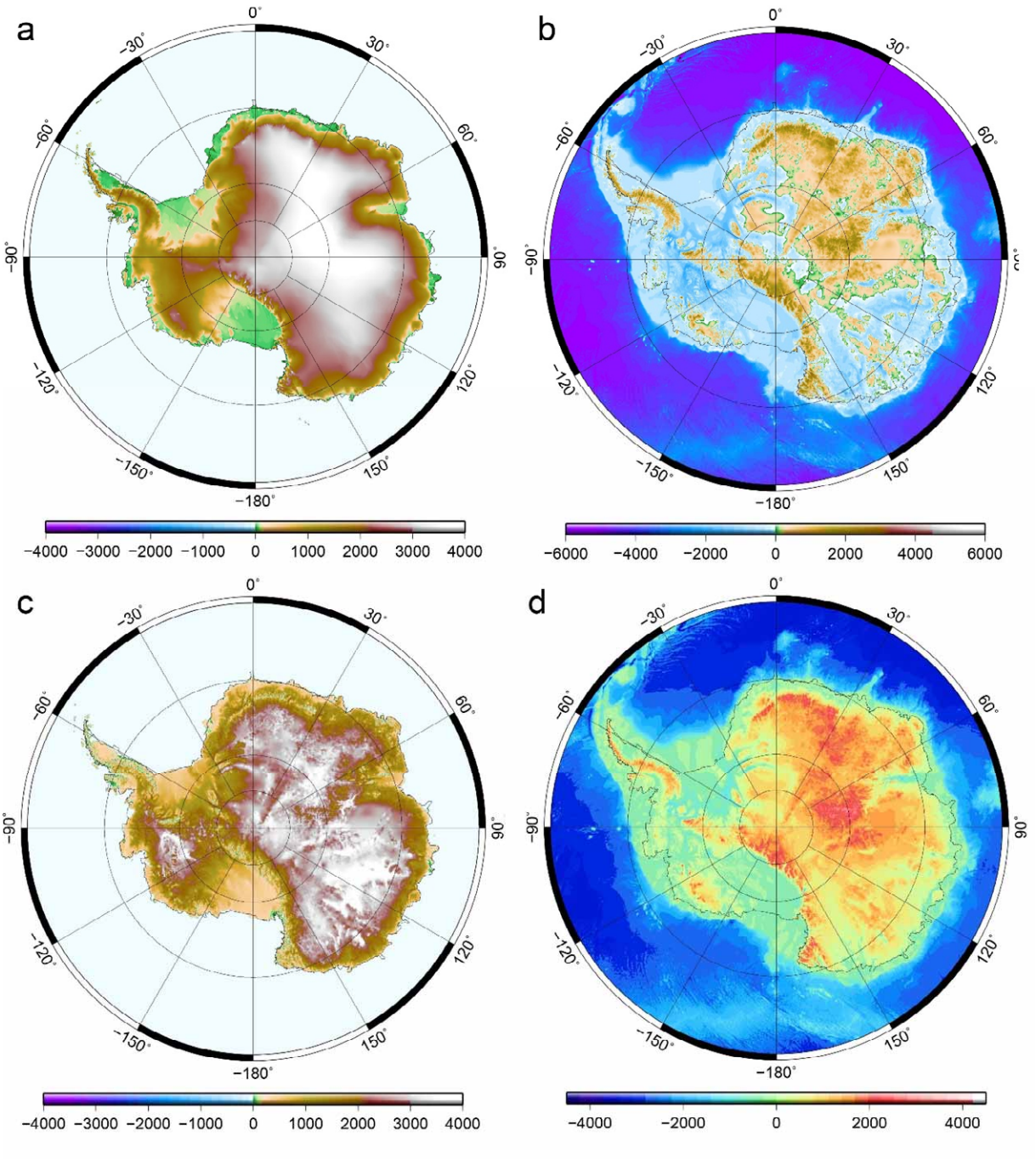

Fig. 3 Earth2014 model components: (a) Surface layer, (b) bedrock, (c) ice sheet thickness, (d) RET2015 rock-equivalent topography, units in m. Panels are in polar-stereographic projection and created with GMT (Wessel et al. 2013)

The Earth2014 1 arc-min global topography model (ddfe.curtin.edu.au/models/Earth2014) is used to describe the topographic masses (ice, water, rock) over Antarctica and elsewhere in this study. Earth2014 is an up-to-date composite model that utilizes Bedmap2 data over continental Antarctica and within a ~450 km offshore zone, SRTM V4.1 (Jarvis et al. 2008) topography from the Shuttle Radar

Topography Mission over land areas within ±60° latitude, Greenland Bedrock Topography v3 (Bamber et al. 2013) and SRTM30_PLUS v9 (Becker et al. 2009) bathymetry over the oceans, major inland lakes and SRTM30_PLUS v9 topography over land areas North of 60° latitude (cf. Hirt and Rexer 2015).

In contrast to Bedmap2 the Earth2014 model is provided in terms of readily usable latitude-longitude grids of global coverage which is a prerequisite for the spherical harmonic modelling techniques applied in Section 3. From the different Earth2014 grid layers, we use the 1-arcmin resolution RET2014 model (Fig. 3d) that describes the masses of land topography, ice sheets, ice shelves, oceans and lakes as rock-equivalent topography (RET, Rummel et al. 1988). In RET2014, the ice and water masses were condensed into equivalent rock layers using a single uniform mass density ρ of 2670 kg m^{-3}. A full account on the construction of Earth2014 and RET2014 is provided by Hirt and Rexer (2015).

In order to benchmark the Bedmap2/Earth2014 added-value for gravity modelling over Antarctica we test the ETOPO1 (Amante and Eakins 2009) global 1-arcmin topography model which relies on the Bedmap1 data set over Antarctica and on various topography data sets outside Antarctica that were available before 2009. The ETOPO1 model comprises two layers (ice surface heights and bedrock) which we use – in direct analogy to the Earth2014 processing – to derive RET over Antarctica and elsewhere (Fig. 4a). A comparison between Bedmap2 and Bedmap1 RET shows significant differences with ~1 km amplitudes in some places (Fig. 4b).

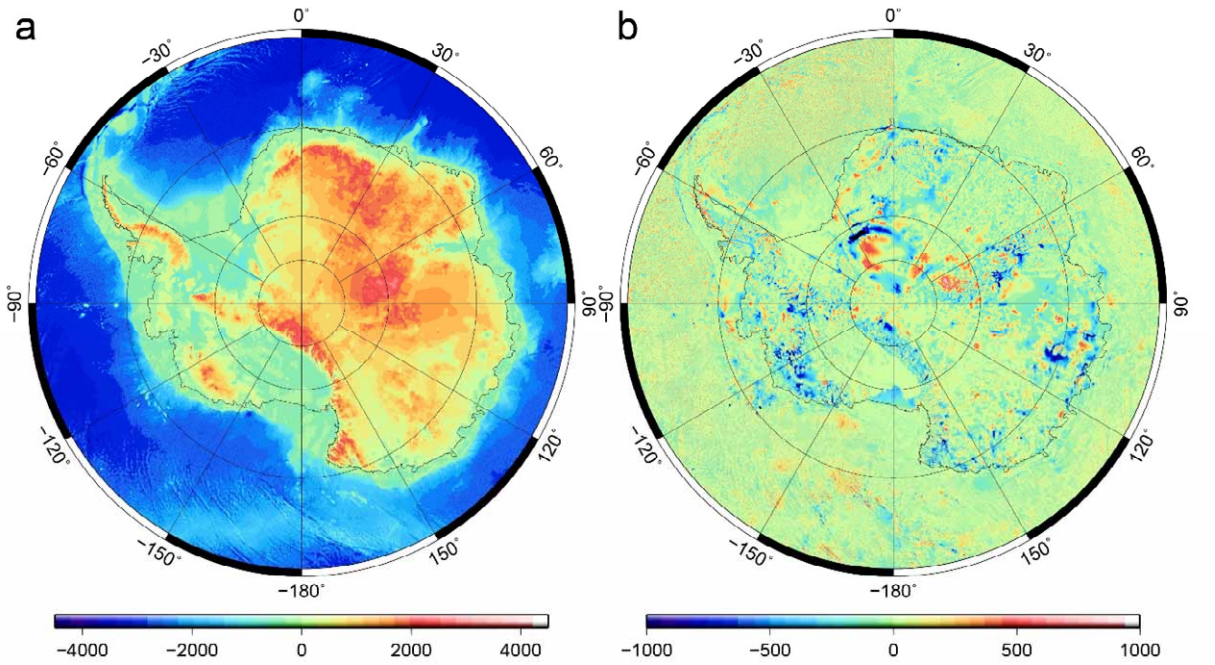

Fig.4 (a) ETOPO1 rock-equivalent topography (RET), (b) differences Earth2014 RET minus ETOPO RET, units in meters

2.3 Airborne gravimetry

For validation of our combined gravity modelling we make use of airborne gravimetry data sets from the AntGG database (Scheinert 2012, Scheinert et al. 2015). A total of six airborne gravimetric surveys were selected (Table 1 and Figure 5). These data sets provide a reasonable geographic coverage of different parts of Antarctica, namely of West Antarctica (data sets #12 (Bell et al., 1999; Studinger et al., 2002), #13 (Luyendyk et al., 2003) and #17 (Diehl et al., 2008)), of transects from the Transantarctic Mountains to the South Pole (#14, Davis 2001; Studinger et al., 2006) respectively to Dome C (#15, Studinger et al., 2004), and of Lake Vostok (#16, Studinger et al., 2003a, 2003b; Holt et al., 2006). With an estimated standard deviation ranging between ~2 and 5 mGal (Scheinert et al. 2015), these data

sets are sufficiently accurate to validate our modelling and benchmark the performance of different modelling variants. Each of the regional surveys comprise some 71,000 to 410,000 airborne gravimetry observations (totalling to more than 1 million observations) covering about ~10% of continental Antarctica. The spacing between parallel flight tracks typically varies between 5 and 15 km which is in good approximation commensurate with the 10 km resolution of our spectral modelling.

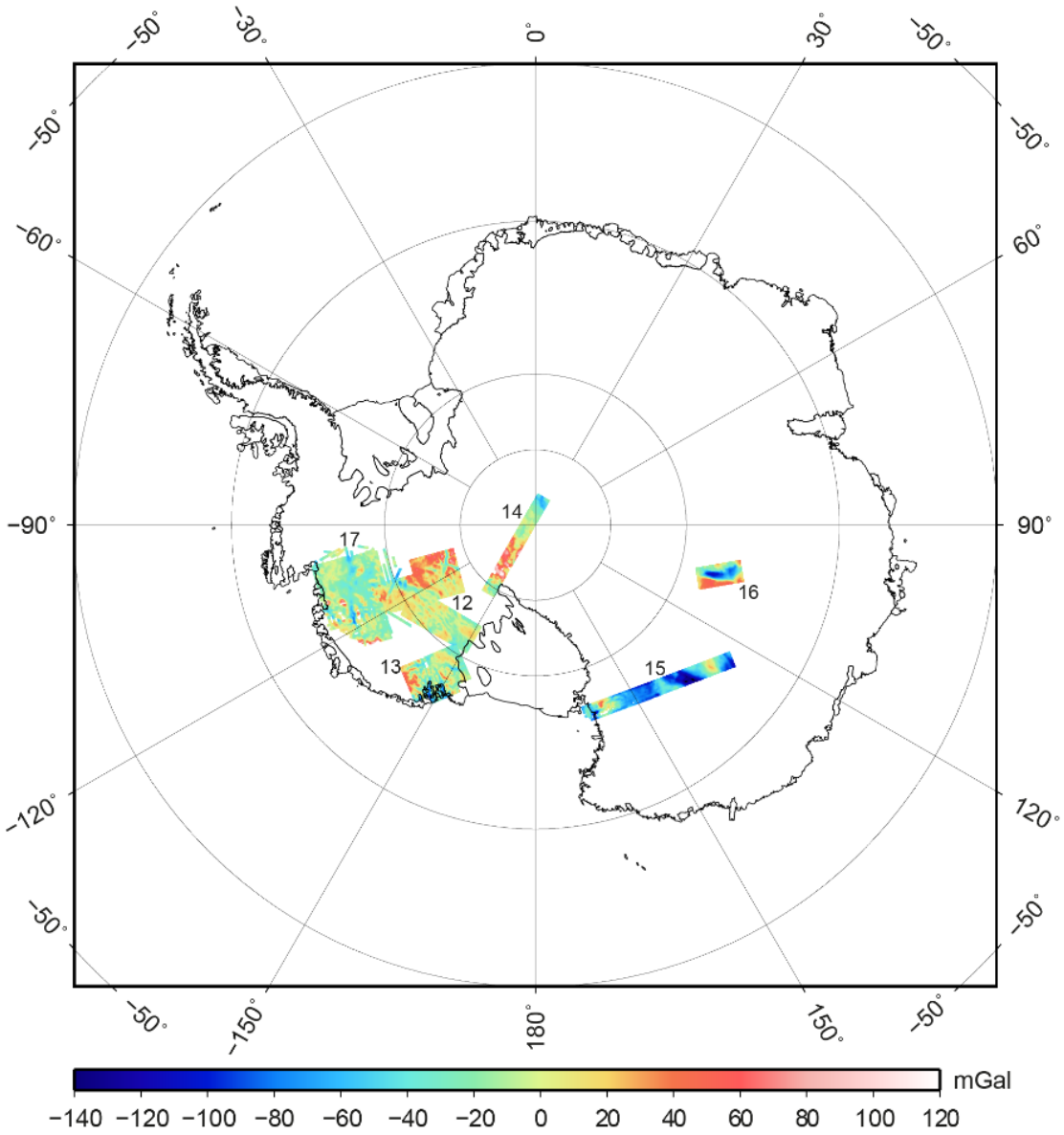

Fig. 5 Data sets from the IAG Subcommission 2.4f "Gravity and Geoid in Antarctica" (AntGG) database (Scheinert et al., 2015) for comparison. Shown are gravity disturbances from six subsets (denoted with 12 to 17) of airborne gravimetry surveys used for validation of global gravity field models. For references to individual data sets see text.

The airborne gravimetry data were continued to the Bedmap2 surface which is consistent with the Earth2014 topographic surface used for the gravity syntheses in this paper (Section 3.3). However, due to a heterogenous or even unknown realization of the gravity datum and due to further effects e.g. when applying downward or upward continuation to a common reference height level, the individual aerogravimetry data sets may contain systematic offsets or even trends. As a result, these data sets may deviate by some constant (bias) from the global models (Section 5). As such, the above standard deviations are valid in a relative sense, rather than specifying the absolute accuracy of the airborne

surveys. However, biases are non-critical for the validation when using simple bias-fit between observations and models.

Table 1. Characteristics of airborne gravimetry data sets from the AntGG database (Scheinert et al., 2015)

Data set identification number	#observations	Approximate location	Estimated accuracy [mGal]
12	411,539	Marie Byrd Land, West Antarctica	3
13	184,600	Western Marie Byrd Land, West Antarctica	5
14	106,820	Transantarctic Mountains – South Pole Transect	3
15	175,158	Transantarctic Mountains – Dome C Transect	2.6
16	144,100	Lake Vostok	1.2
17	70,764	Eastern Marie Byrd Land, West Antarctica	2.3

3 Methods

3.1 Topographic potential

The topographic potential generated by the topographic masses (rock, ice, water) is computed with the harmonic combination (HC) method (Claessens and Hirt 2013). The HC-method is a spectral-domain gravity forward modelling technique that delivers the topographic potential in ellipsoidal approximation (i.e., field-generating masses are arranged on the surface of a reference ellipsoid). We use the RET2014 (Section 2.2) rock-equivalent topography at 2 arc-min resolution (downsampled from 1 arc-min with 2x2 box means) as input to describe the topographic masses, and the GRS80 ellipsoid with its geometry parameters semi-major axis a and semi-minor axis b as reference. In the first step, RET2014 heights $\mathrm{H_{RET2014}}$ are used to compute the (dimensionless) topographic height function H

$$H = \frac{H_{RET2014}}{r_e}. \quad (1)$$

The ellipsoidal radius $\mathrm{r_e}$ is obtained as a function of the geocentric latitude φ via (Claessens 2006)

$$r_e(\varphi) = a\sqrt{\frac{1-e^2}{1-e^2 cos^{\,2}\varphi}} \quad (2)$$

where e^2 is the first numerical eccentricity squared. In the second step, H is analysed harmonically, yielding fully-normalized SHCs $\overline{H}_{nm} := (\overline{HC}_{nm}, \overline{HS}_{nm})$ of degree n and order m which can be used to evaluate the harmonic series

$$H(\varphi,\lambda) = \sum_{n=0}^{n_{max}} \sum_{m=0}^{n} \left(\overline{HC}_{nm}\, cos\, m\lambda + \overline{HS}_{nm}\, sin\, m\lambda\right) \bar{P}_{nm}(sin\,\varphi) \quad (3a)$$

with $\bar{P}_{nm}(\sin\varphi)$ denoting the fully-normalized Associated Legendre Functions of degree n and order m, λ being the longitude and φ the geocentric latitude of the computation point, and n_{max} the maximum harmonic degree. Third, integer powers $\mathrm{H^{(p)}}$ of the topographic height function H (from Eq. 3a, evaluated to n_{max} =2160) are formed with power p running from 1 to 10. The $H^{(p)}$ grids are analysed harmonically, yielding fully-normalized SHCs $\overline{H}_{nm}^{(p)} := (\overline{HC}_{nm}^{(p)}, \overline{HS}_{nm}^{(p)})$ of the harmonic series

$$H'^{(p)}(\varphi,\lambda) = \sum_{n=0}^{n_{max}} \sum_{m=0}^{n} \left(\overline{HC}_{nm}^{(p)} \cos m\lambda + \overline{HS}_{nm}^{(p)} \sin m\lambda \right) \bar{P}_{nm}(\sin\varphi) \qquad (3b)$$

Note that $H'^{(p)}$and $H^{(p)}$ are usually not identical unless $H^{(p)}$ is a function band-limited to n_{max} (cf. Hirt and Kuhn 2014).

In a second step, we use the sets of SHCs $H_{nm}^{(p)}$ to compute the topographic potential in spherical harmonics via (Claessens and Hirt 2013)

$$\bar{V}_{nm} = \frac{4\pi\rho b^3}{M(2n+1)(n+3)} \left(\frac{b}{R}\right)^n \sum_{p=1}^{n+3} \binom{n+3}{p} \sum_{j=0}^{Jmax} (-1)^j \binom{-\frac{n+3}{2}}{j} e^{2j} \sum_{i=-j}^{j} \bar{K}_{nm}^{2i,2j} \bar{H}_{n+2i,m}^{(p)} \qquad (4)$$

where ρ is the mass-density of the RET2014 topographic masses, M is Earth's mass, b is the semi-minor axis of the reference ellipsoid and R is the scaling factor for the topographic potential coefficients. $\bar{V}_{nm}$ is the short-hand for the topographic potential coefficients ($\overline{VC}_{nm}$, $\overline{VS}_{nm}$) and variable $\bar{K}_{nm}^{2i,2j}$ denotes fully-normalized sinusoidal Legendre weight functions (short: weights), cf. Appendix A for their computation. The set of $\bar{V}_{nm}$ coefficients which describe the topographic potential – as implied by RET2014 – in ellipsoidal approximation is denoted the dV_ELL_RET2014 topographic potential model.

In Eq. (4), each (solid) topographic potential coefficient $\bar{V}_{nm}$ is computed as a combination of weighted (surface) $H_{nm}^{(p)}$ – coefficients of equal order *m* ("*harmonic combination*"). The innermost summation over variables *i* and *j* are the result of applying a binomial series expansion to the attenuation factor in the derivation of Eq. (4), see Claessens (2006) and Claessens and Hirt (2013) for details. While these innermost summations must be theoretically carried out to infinity, the series have been found to sufficiently converge if truncated at a maximum summation index of $Jmax$ = 30 (Claessens and Hirt 2013). As a result of this procedure, each topographic potential coefficient $\bar{V}_{nm}$ is computed as a function of 60 products $\bar{K}_{nm}^{2i,2j} \bar{H}_{n+2i,m}^{(p)}$. Hence, there is no degree-to-degree relation between $\bar{V}_{nm}$ and $H_{nm}^{(p)}$. Instead, each potential coefficient $\bar{V}_{nm}$ depends on all $H_{nm}^{(p)}$- coefficients within a narrow spectral band comprising the harmonic degrees *n-30 to n+30.*

The described procedure gives rise to some additional coefficients in spectral band of degrees 2161 to 2190, even when limiting all $H_{nm}^{(k)}$ to $n_{max} = 2160$. This is akin to the EGM2008 (Pavlis et al. 2012) geopotential model which is band-limited to degree 2160 in ellipsoidal harmonics, while its spherical harmonic representation (derived with the Jekeli (1988) method) features additional coefficients in the spectral band 2161-2190. The importance of including these additional high-degree coefficients in the synthesis is emphasized here; truncation of the $\bar{V}_{nm}$ set of coefficients at degree 2160 gives rise to spurious artefacts over the Polar Regions (Section 4.2) and is not recommended.

3.2 Merging of satellite and topography data

3.2.1 Merging GRACE and GOCE data

Key input for the least-squares combination of the GRACE and GOCE GGMs are the normal equations

$$N_{GOCE} = (A^T P A)_{GOCE} \tag{5a}$$

$$N_{GRACE} = (A^T P A)_{GRACE} \tag{5b}$$

and the vectors of weighted observations

$$n_{GOCE} = (A^T P l)_{GOCE} \tag{6a}$$

$$n_{GRACE} = (A^T P l)_{GRACE} \tag{6b}$$

where l are the observations, P the weighting matrix and A the design matrix. We use the pre-computed N-matrices and n-vectors for GRACE (Mayer-Gürr et al. 2010) and for GOCE (Brockmann et al. 2014). For a least-squares combination of both models, the normal equations and vectors of weighted observations are added

$$[N_{GOCE} + N_{GRACE}]\, x_{sat} = [n_{GOCE} + n_{GRACE}] \tag{7a}$$

$$\Updownarrow$$

$$N_{sat}\, x_{sat} = n_{sat} \tag{7b}$$

where x_{sat} is the vector of (unknown) spherical harmonic coefficients, N_{sat} is the normal equation and n_{sat} is the corresponding vector of weighted observations l of the combined satellite-only model GRACE/GOCE-2014 (abbreviated to GG14). Both satellite normal equation systems rely on realistic stochastic modelling (utilizing variance-covariance information, cf. Pail et al. (2011), Brockmann et al. (2014)). Therefore, the systems can be combined using the unit weight. This has been corroborated by variance component estimation where the variance components were found to be close to 1 (cf. Fecher et al. 2015). This satellite-only solution x_{sat} (obtained from Eq. 7b through left-multiplication with N_{sat}^{-1}) has the same spectral resolution as GOCE-TIM5 (degree 280), but is free of any constraints (like Kaula's rule) while reinforced by GRACE-information at long/medium wavelengths. The relative contributions (redundancy numbers, computed with full variance-covariance information) of GRACE to GG14 are displayed in Fig. 6a and the power spectrum of GG14 is shown in Fig. 7. Note the rise in spectral energy in spectral band of degrees 240-280 which is a sign of missing regularization in GG14. The deficiencies of the GG14 combination (besides the unrealistic short-scale spectral energy (cf. Fig. 1) also the weakly determined near-zonal coefficients) are "rectified" to some extent in the subsequent regularization with aid of the topographic potential model dV_ELL_RET2014 (Section 3.2.2).

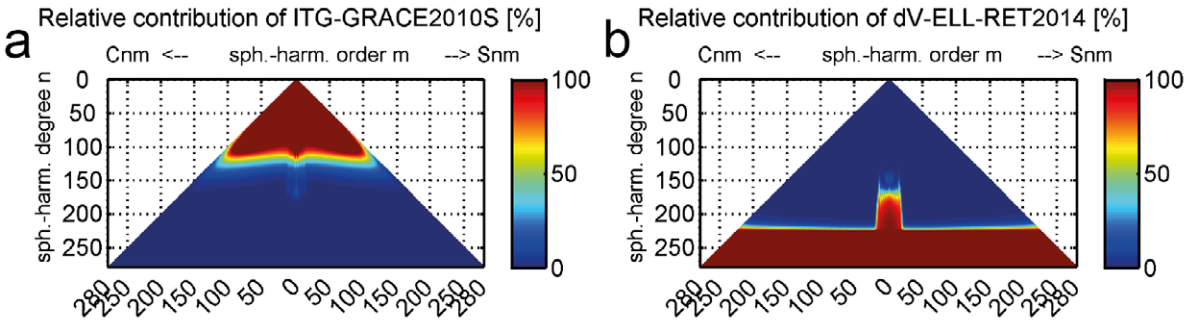

Fig. 6 Relative contribution of GRACE (and GOCE, respectively) to the combined satellite-only model GG14 (left), and relative contribution of dV_ELL_RET2014 (and GG14, respectively) to the satellite-topography-combined SatGravRET2014 model (right)

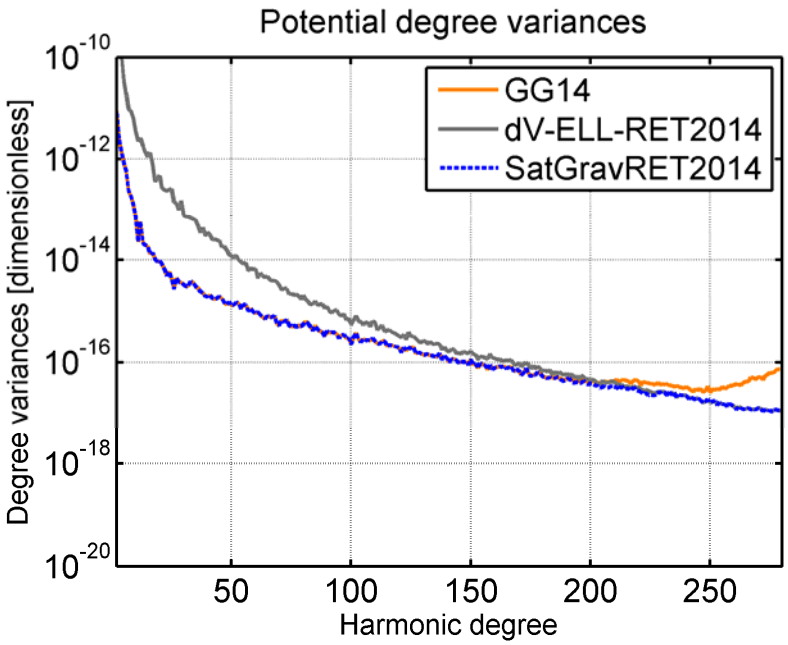

Fig. 7 Dimensionless potential degree variances of the satellite-only model GG14 (GRACE and GOCE) in orange, of the topographic potential model dV_ELL_RET2014 (in grey) and of the combined model SatGravRET2014 (in blue). Note that the orange curve closely follows the blue one to about degree ~200, and the grey curve is very close to the blue beyond degrees 230.

3.2.2 Merging GG14 with dV_ELL_RET2014

Next we merge the satellite-only GG14 solution with the dV_ELL_RET2014 topographic potential model, yielding the combined SatGravRET2014 potential model. In this step, the coefficients of dV_ELL_RET2014 are used to regularize the GG14 model, i.e., stabilize their short-scale spectral energy behaviour. That means, the dV_ELL_RET2014 $\mathrm{x}_{\mathrm{RET2014}}$ coefficients (which are treated as a priori known) and their variances (not known, therefore defined empirically as described later) are incorporated into the right-hand side and into the diagonal of normal equation matrix, following

$$(N_{sat} + \Sigma(x_{RET2014})^{-1})\ x = n_{sat} + \Sigma(x_{RET2014})^{-1}\ x_{RET2014} \qquad (8a)$$

$$\Updownarrow$$

$$\left(N_{sat} + N_{\mathrm{topo}}\right)\ x = n_{sat} + n_{topo} \qquad (8b)$$

where x denotes the optimally combined set of SHCs from ITG-GRACE2010s, GOCE TIM5 and dV_ELL_RET2014 in least-squares sense. The terms N_{topo} and n_{topo} are the normal equation matrix and the corresponding right-hand side, respectively, of the normal equation system of dV_ELL_RET2014. We use the Jacobian matrix as the identity matrix and the variance-covariance matrix $\Sigma(x_{RET2014})^{-1}$ (and thus the normal equation matrix itself) as a diagonal matrix. The diagonal contains the inverse variance of each coefficient.

Crucially, the inverse variances of the coefficients of dV_ELL_RET2014 serve as weights in the least squares process that define the relative impact in the combination with GG14. As such, the role of the weights assigned to the dV_ELL_RET2014 coefficients is to “control” the combination of satellite and topographic potential.

Note, that during the computation of the topographic potential coefficients (Section 3.1) variance information is not estimated and, therefore, has to be generated empirically. We have designed three different weighting schemes A, B and C for the topographic potential (see Table 2 for details) with the

transition between the satellite-only model and the topographic potential model occurring mainly in the spectral band of degrees ~210 to ~240. The specific standard deviations of scheme A for dV_ELL_RET2014 (with the transition band from degrees 210 – 225) are shown together with those from GG14 (as obtained from N_{sat}^{-1}) in Fig. 8.

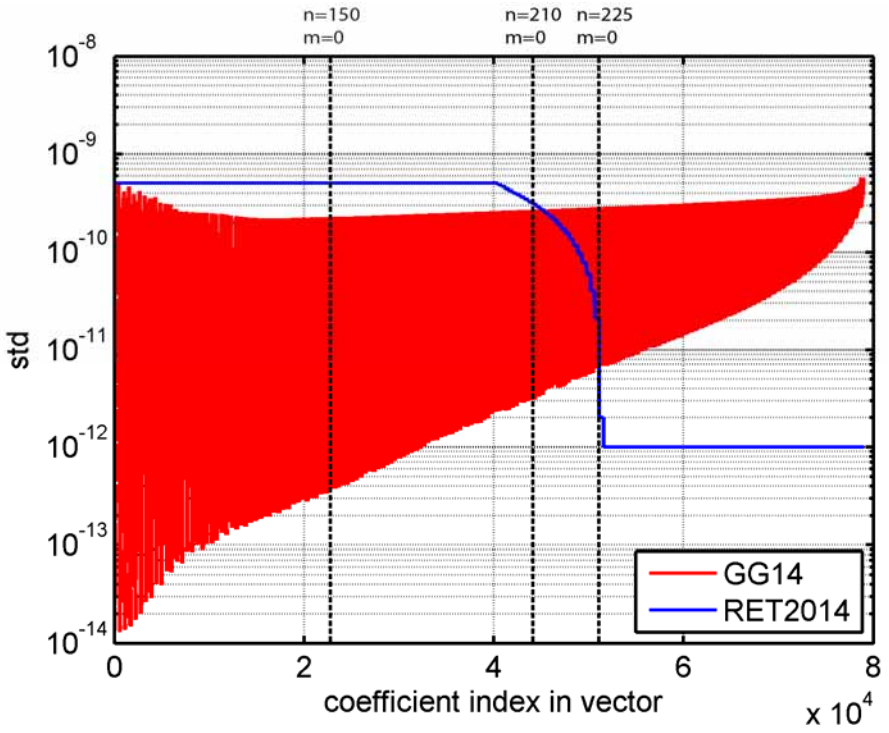

Fig 8. Designed standard deviations of weighting scheme A for dV_ELL_RET2014 (blue) together with the estimated standard deviations for the satellite-only solution GG14 (red) per index. Coefficient ordering is as follows: $C_{00}, C_{10}, C_{11}, S_{11}, C_{20}, C_{21}, C_{22}, S_{21}, S_{22}, (\ldots)$.

The relative contribution of the satellite-only and topographic potential to the SatGravRET2014 combination, as given by the relation of the variance information of each input model and the combined model, reveals that the topographic potential model becomes increasingly dominant in the band of degrees 210 to 225 for coefficients of order > ~25 (Fig. 6b). In the near-zonal coefficient group (m< ~25) the topographic potential already comes into play around degree 150 and makes a contribution of more than 50% beyond degree ~170. This behaviour is to be explained by the relatively weak determination of the near-zonal coefficients (large variances of low-order coefficients) based on GOCE gradient observations due to the satellite's polar observation gaps as a result of its orbit inclination. In other words, the polar Regions are stabilized (filled with forward-modelled information) already at spatial scales of ~130 km while outside this region forward-modelling provides information at scales shorter than ~95 km.

A last step to obtain a usable gravity field model is to exchange the J2 (C20) coefficient of the newly combined model with a better one. Due to different reasons, the GRACE mission cannot be used to accurately determine the oblateness of Earth's gravity field (which is captured in J2). Therefore, we use the rescaled equivalent from the combined satellite gravity model GOCO03s (Mayer-Gürr et al. 2012):

$$J_{2_{scaled}} = J_{2_{GOCO03s}} \cdot \left(\frac{GM_{RET2014}}{GM_{GOCO03s}}\right) \cdot \left(\frac{a_{RET2014}}{a_{GOCO03s}}\right)^2 = -4.841651993008015 \cdot 10^{-4} \quad (9)$$

The described combination procedure was applied with three differently designed weighting schemes (Table 2) changing the impact of GG14 in the combination, and with topographic potential coefficients computed from ETOPO1-rock equivalent topography instead of RET2014 (section 3.1). This yields the SatGravETOPO1 geopotential model. An overview of all computed potential models is given in Table 2. The different weighting schemes (A-C) and the two sources of topographic mass information (ETOPO1 vs. RET2014) allow us to test a range of solutions against the terrestrial gravity observations.

Table 2. Specifications of six combined gravity models generated in this study, and weighting schemes applied (spectral transition range, in harmonic degrees)

Combination model name	Normal equation input	Regularization Input	Spectral transition range
SatGravRET2014_A	GG14	dV_ELL_RET2014	210 – 225
SatGravRET2014_B	GG14	dV_ELL_RET2014	212 – 231
SatGravRET2014_C	GG14	dV_ELL_RET2014	215 – 240
SatGravETOPO1_A	GG14	dV_ETOPO1_RET	210 – 225
SatGravETOPO1_B	GG14	dV_ETOPO1_RET	212 – 231
SatGravETOPO1_C	GG14	dV_ETOPO1_RET	215 – 240

3.3 Accurate computation of gravity field functionals

The derived sets of SHCs were used to synthesize gravity disturbances δg and quasigeoid heights ζ at the surface of the topography $H = H_{SUR2014}$, as represented by the Earth2014 SUR surface layer (Fig. 3a). Synthesis at the surface of the topography (also known as 3D-synthesis), rather than at the ellipsoidal surface is crucially important for accurate gravity modelling, given Antarctica's topographic surface is often 2-4 km above the mean sea level. Considering topographic heights in the synthesis takes into account the effect of gravity attenuation with elevation (Hirt and Kuhn 2014) and is mandatory if the gravity field functionals synthesized from the GGM are to be used as accurate predictions for observed values, particularly from high-degree global models (Hirt 2012).

For efficient 3D synthesis we applied the gradient continuation approach as described in Hirt (2012) and implemented in Bucha and Janak's (2014) isGrafLab software. As basic idea of the gradient approach, high-resolution grids of the gravity field functional and its radial derivatives (to higher order) are computed at some mean reference height and used for field continuation to the (irregularly shaped) topographic surface with Taylor series expansions (Holmes 2003). Although this method is approximative, it is sufficiently accurate (see below) in view of the overall uncertainties of the forward modelling (Section 5) while being numerically highly-efficient (see Holmes 2003, Hirt 2012, Bucha and Janak 2014). The 3D-SHS method used here are based on continuation along the radial direction, and not along the ellipsoidal normal, which would be more accurate (Bucha and Janak 2014). The maximum approximation errors associated with radial continuation are at the level of few 0.1 mGal for gravity disturbances and few 0.1 mm for quasigeoid heights from degree-2190 expansions which we consider safely negligible relative to the uncertainties inherent in the gravity forward modelling (Section 5).

We note that continuation techniques were used in the context of the EGM2008 development too, both for the analytical downward continuation (Pavlis et al. 2012, p.7 ibid) and - although less documented in the literature - for the computation of EGM2008 geoid height grids which rely on gravity and height anomalies synthesized on a digital topography with 3D-synthesis methods.

We start by synthesizing *k*-th-order radial derivatives of gravity disturbances $\delta g_{r(k)}$

$$\delta g_{r(k)}(\varphi,\lambda,r_e+H_{ref}) = (-1)^k \frac{GM}{r^{k+2}} \sum_{n=2}^{n_{max}} (n+1) \left\{ \prod_{i=1}^{k} (n+i+1) \right\} \left(\frac{a}{r}\right)^n \cdot \sum_{m=0}^{n} ((\overline{VC}_{nm} \cos m\lambda \;\; \overline{VS}_{nm} \sin m\lambda)\, \bar{P}_{nm}(\sin\varphi) \tag{10}$$

and of quasigeoid heights $\zeta_{r(k)}$

$$\zeta_{r(k)}(\varphi,\lambda,r_e+H_{ref}) = (-1)^k \frac{GM}{r^{k+1}\gamma} \sum_{n=2}^{n_{max}} \left\{ \prod_{i=1}^{k} (n+i+1) \right\} \left(\frac{a}{r}\right)^n \cdot \sum_{m=0}^{n} ((\overline{VC}_{nm} \cos m\lambda \;\; \overline{VS}_{nm} \sin m\lambda)\, \bar{P}_{nm}(\sin\varphi) \tag{11}$$

with *k* ranging from 0 to 5 (the 0th-order radial derivative is the functional itself), and using the geocentric latitude φ, longitude λ and $r = r_e + H_{ref}$ as geocentric radius of the computation points *P*. The sum of H_{ref} (reference height, here 2000 m) and r_e (ellipsoidal radius, Eq. 2) is constant along parallels, allowing to use fast algorithms by Holmes and Featherstone (2002). The computation points $P(\varphi,\lambda,r_e+H_{ref})$ are arranged in densely spaced cell-centred grids (2 arc-min resolution) covering the whole of Antarctica ($-90° < \varphi < -60°, -180° < \lambda < 180°$).

Gravity disturbances $\delta g(\varphi,\lambda,r_S)$ at the surface of the topography are then obtained through applying the Taylor series expansion

$$\delta g(\varphi,\lambda,r_S) \approx \sum_{k=0}^{k_{max}} \frac{1}{k!} \delta g_{r(k)}(\varphi,\lambda,r_e+H_{ref}) \cdot (H-H_{ref})^k \tag{12}$$

where k_{max} = 5 is the maximum order, $(H-H_{ref})$ are the topographic heights of the surface points relative to H_{ref}, and $r_S \approx r_e + H$ is the geocentric radius of the surface points. Quasigeoid heights $\zeta(\varphi,\lambda,r_S)$ are computed via

$$\zeta(\varphi,\lambda,r) \approx C_{1B}(\varphi,\lambda,r) + \sum_{k=0}^{k_{max}} \frac{1}{k!} \zeta_{r(k)}(\varphi,\lambda,r_e+H_{ref}) \cdot (H-H_{ref})^k \tag{13}$$

Where the C_{1B}-term (Rapp 1997, modified through Hirt 2012)

$$C_{1B}(\varphi,\lambda,r) = \frac{\partial\zeta}{\partial\gamma}\frac{\partial\gamma}{\partial h}\Big|_{r_e+H_{ref}} (H-H_{ref}) \tag{14}$$

$$\approx \frac{-\zeta_{(0)}(\varphi,\lambda,r_e+H_{ref})}{\gamma(\varphi,h_{ref})} (-3.086\ 10^{-6}\ \mathrm{s}^{-2})(H-H_{ref})$$

takes into account the effect of the change in normal gravity γ between H and H_{ref} in the computation of $\zeta_{r(k)}$ in Eq. (11). For the computation of the normal gravity, where ellipsoidal heights are required, the use of $h_{ref} \approx H_{ref} + \zeta_{(0)}$ is sufficient.

4 Results

The main outcomes of this study are (i) the SatGravRET2014 spherical harmonic model expressed through its set of SHCs to degree 2190, and (ii) high-resolution (2-arcmin) grids of synthesized gravity disturbances and height anomalies which we compare with selected models and gravity observations. Unless stated otherwise all synthesized gravity functionals refer to the Earth2014 topographic surface used in the 3D-SHS (Section 3.3), and all combined solutions are based on the A-weighting scheme (Table 2).

4.1 Space domain

Gravity disturbances

Figure 9 compares gravity disturbances from EGM2008 (entirely relying on GRACE satellite gravimetry over continental Antarctica), GOCE-TIM5 satellite-only model, our new combined SatGravRET2014 model, and from the dV_ELL_RET2014 topographic potential model. An increase in spatial resolution from GRACE (Fig. 9a, effective resolution to degree ~160) to GOCE satellite gravimetry (Fig. 9b, effective resolution to about degree ~240) is visible, corresponding to factor ~1.5. The SatGravRET2014 model enhances the GRACE/GOCE resolution by a factor of ~8 to degree 2190, or from ~80 km to ~10 km spatial scales (Figures 9b vs. 9c).

For comparison, gravity disturbances from the topographic potential model dV_ELL_RET2014 are displayed, too (Fig. 9d). The combination procedure (Section 3.2) effectively substitutes the long- and medium wavelength constituents of the topographic gravity field (Fig. 9d) by observed information from satellite gravimetry (Fig. 9a,b), yielding the combined model shown in Fig. 9c. Fig. 10a displays the short-scale (spectral band of degrees 226 to 2190) constituents of the SatGravRET2014 model, which possess a RMS (root-mean-square) signal strength of ~21 mGal and reach maximum amplitudes in excess of 250 mGal (cf. Table 3). It is these short-scale gravity signals which are not represented yet by recent high-degree geopotential models such as EGM2008 and EIGEN-6C4 over continental Antarctica, but modelled here from high-resolution Bedmap2 topography, ice and bedrock data. The RMS signal strength of the GOCE-TIM5 model is about ~37 mGal over continental Antarctica, suggesting that the Bedmap2-delivered short-scale gravity signals (Fig. 10a) reach about 50 % strength of those captured by tnhe GRACE and GOCE satellite-missions (Fig. 9a,b). This is not surprising, bearing in mind that the spectral energy of gravity disturbances (as radial derivative of the potential) is significant at all spatial scales (e.g., Torge and Müller 2014).

Quasigeoid heights

Fig. 11 (panel a) shows the quasigeoid heights from the SatGravRET2014 model over the Antarctic region, varying within a range of ~100 m (Table 4). The C1B-term (Eq. 14) included in the quasigeoid heights reaches in our case (reference height of 2000 m) RMS values of 2 cm and maximum values of 6 cm (Fig. 11b and Table 4), so is relevant for accurate quasigeoid computation through 3D-SHS. In analogy to Fig. 10a, the short-scale Bedmap2-implied quasigeoid signals are shown in Fig. 10b. The RMS signal strength of the SatGravRET2014 model constituents in band 226 to 2190 is ~35 cm with amplitudes of about 3 m (Table 4). These numbers are consistent with previous findings by Scheinert et al. (2008) and Flury and Rummel (2005). Scheinert (2008) reported quasigeoid signals reaching ~3m amplitudes beyond the resolution of satellite gravimetry models, and Flury and Rummel (2005) estimated mean quasigeoid signal strengths of ~28 cm (beyond harmonic degree 300). These numbers suggest that satellite-only quasigeoid heights, even from the recent GOCE mission, limit the achievable accuracy of GNSS-based height transfer to the level of 0.3-0.4 m over Antarctica. This is commensurate with estimates obtained from Morgan and Featherstone (2009) who estimated the accuracy of EGM2008 over East Antarctica based on tide-gauge data sets.

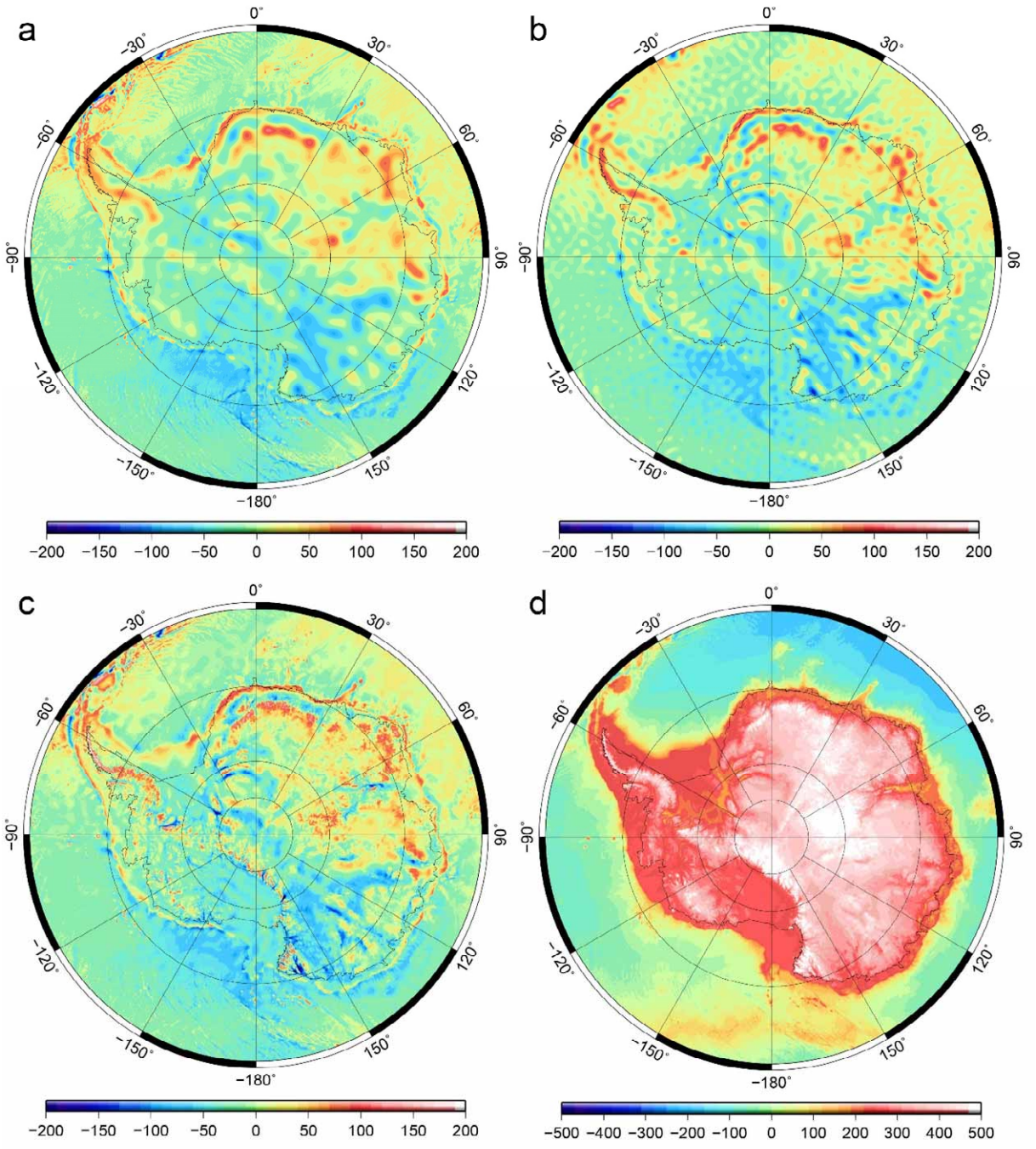

Fig. 9 Gravity disturbances evaluated at the Earth2014 topographic surface from (a) EGM2008 in band 2 to 2190, (b) GOCE-TIM5 in band 2 to 280, (c) SatGravRET2014_A in band 2 to 2190 and (d) topographic potential model dV_ELL_RET2014 in band 2 to 2190. Unit in mGal (10^{-5} m s^{-2}). The large signal amplitudes associated with the topographic potential model dV_ELL_RET2014 reflect the effect of unmodelled isostatic mass compensation (relevant at long and medium wavelengths).

Table 3. Descriptive statistics of gravity disturbances from various models in different spectral bands over continental Antarctica, unit in mGal

Model	Band	Min	Max	Mean	RMS	STD
EGM2008	2 to 2190	-104.0	218.0	-6.8	34.8	34.1
GOCE-TIM5	2 to 280	-148.0	114.0	-6.8	37.9	37.3
dV_ELL_RET2014	2 to 2190	67.0	672.0	351.1	360.3	81.1

SatGravRET2014_A	2 to 2190	-258.0	289.0	-6.7	42.7	42.2
SatGravETOPO1_A	2 to 2190	-239.0	299.0	-6.7	41.4	40.9
SatGravRET2014_A minus SatGravETOPO1_A	2 to 2190	-122.0	116.0	0.0	12.8	12.8
SatGravRET2014_A	226 to 2190	-251.0	281.0	0.1	20.9	20.9
SatGravRET2014_A	2161 to 2190	-138.0	144.0	-0.0	17.2	17.2

Table 4. Descriptive statistics of quasigeoid heights and in different spectral bands, and of the C1B correction term over continental Antarctica, unit in meters

Model or term	Band	**Min**	**Max**	**Mean**	**RMS**	**STD**
SatGravRET2014_A	2 to 2190	-60.96	36.76	-14.44	28.52	24.59
SatGravRET2014_A	226 to 2190	-2.68	3.27	0.00	0.35	0.35
SatGravRET2014_A	2161 to 2190	-0.41	0.43	-0.00	0.05	0.05
C1B-term	2 to 2190	-0.03	0.06	0.01	0.02	0.02

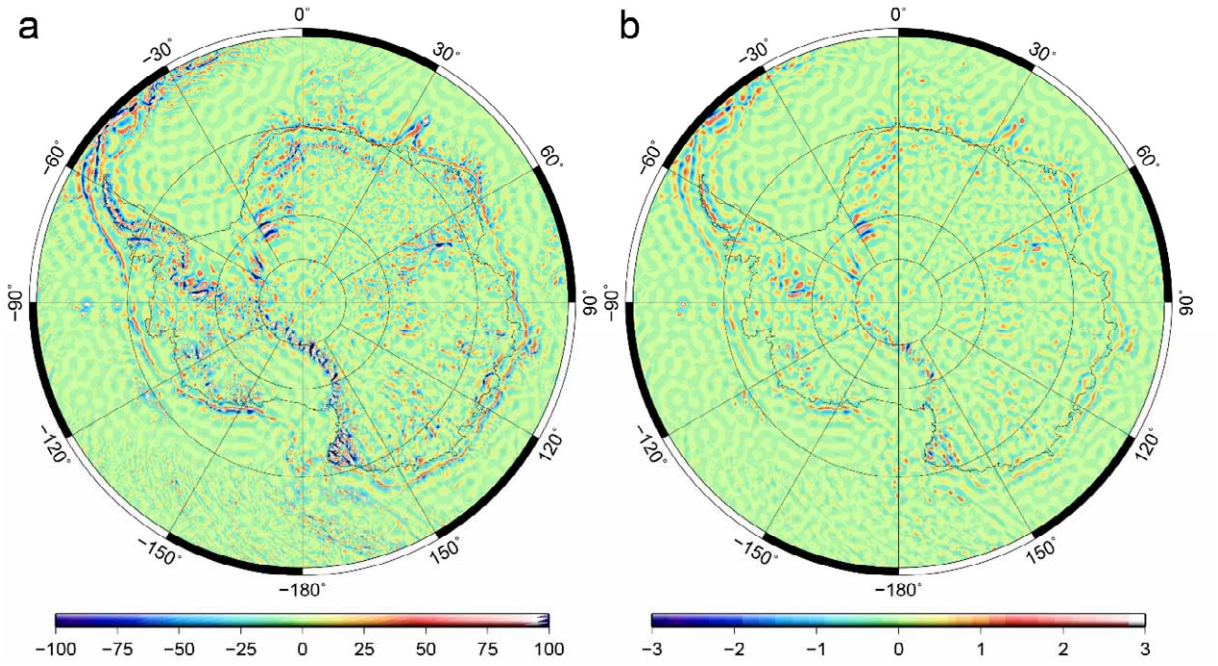

Fig. 10 Short-scale gravity field signals in spectral band of degrees 226 to 2190 from SatGravRET2014_A. Panel a: Gravity disturbances (unit in mGal), Panel b: Quasigeoid heights (unit in meters). Functionals evaluated at the Earth2014 topographic surface with 3D spherical harmonic synthesis.

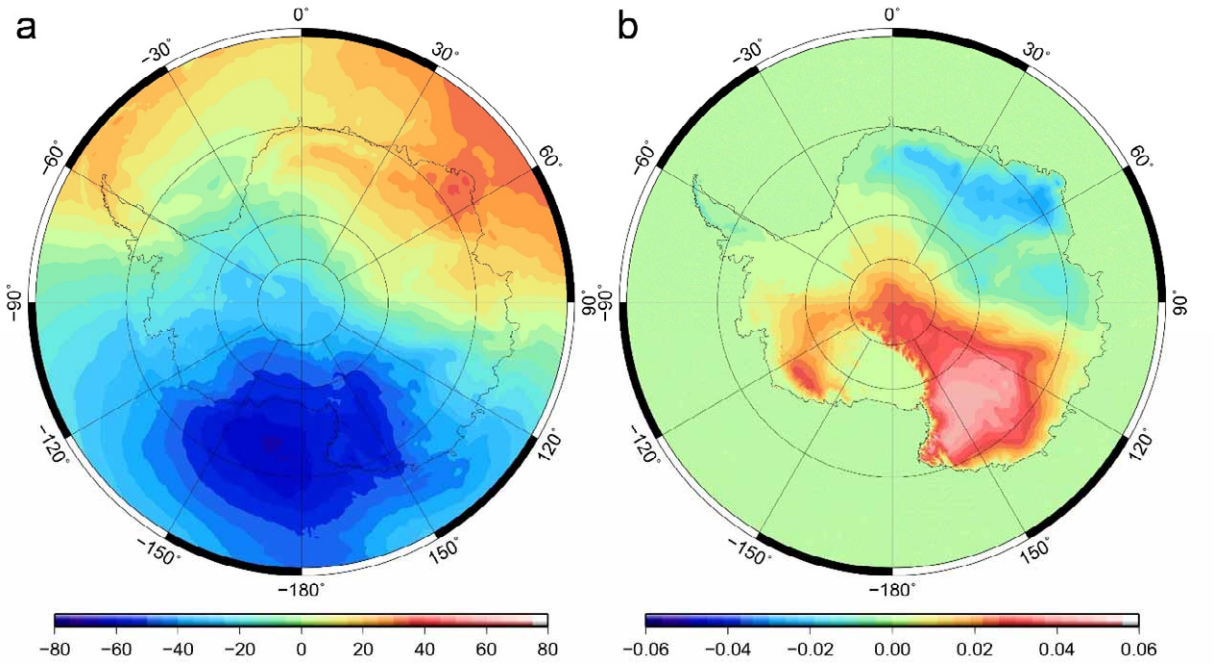

Fig. 11 Quasigeoid heights evaluated at the Earth2014 topographic surface from (a) SatGravRET2014_A in band 2 to 2190, and (b) C1B correction term (reference height 2000 m above the GRS80 ellipsoid), unit in meters.

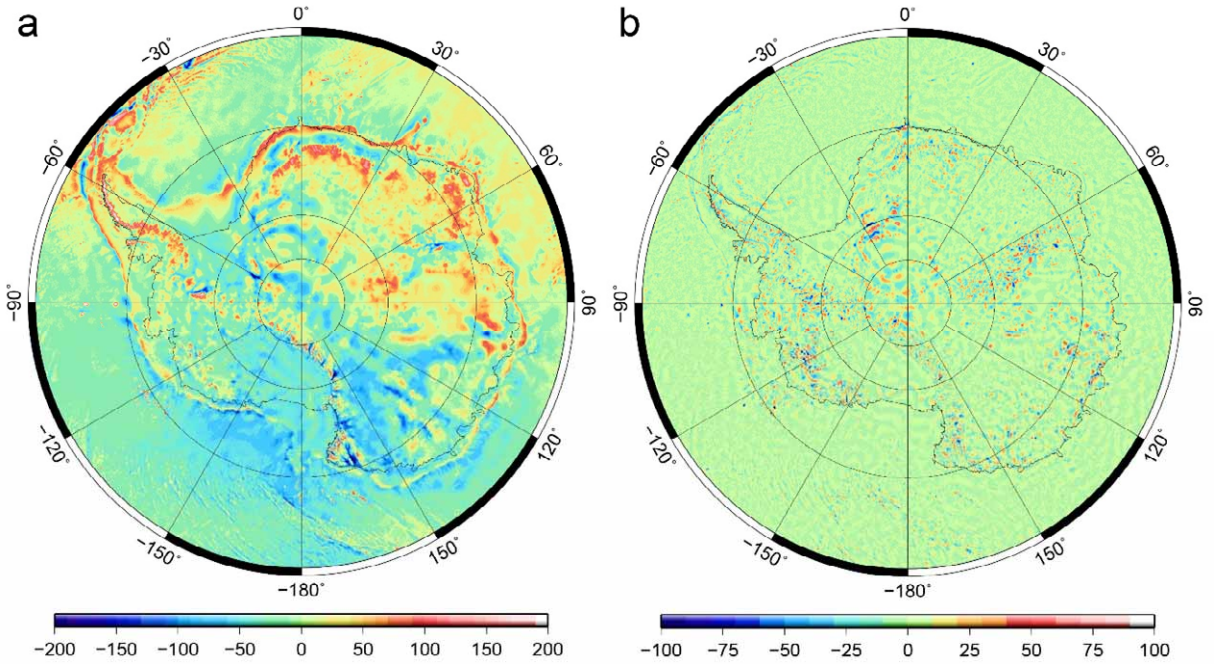

Fig. 12 Gravity disturbances evaluated at the Earth2014 topographic surface from (a) SatGravETOPO1_A in band 2 to 2190, and (b) gravity disturbance differences SatGravRET2014_A minus SatGravETOPO1_A, unit in mGal.

Bedmap2 vs. Bedmap1

We compared gravity disturbances from the SatGravETOPO1 model (based on Bedmap1 instead of Bedmap2, cf. Section 2.2) against those from SatGravRET2014. From Fig. 12 and Table 3, the differences in gravity disturbances frequently exceed ~50 mGal (maximum ~120 mGal, RMS at the 10 mGal level), mostly over regions where new ice thickness measurements were incorporated into Bedmap2 (cf. Fretwell et al. 2013). As such Fig. 12 (panel b) shows how the discrepancies between rock-equivalent heights from the Bedmap2 and Bedmap1 compilations (Fig. 4b) translate into gravity

effects. Because GRACE and GOCE data was equally used in the SatGravRET2014 and SatGravETOPO1 models, the long/medium-wavelength discrepancies in Fig. 4b do not play a role, instead only the short-scale (beyond harmonic degree 226) RET-height differences between Bedmap2 and Bedmap1 propagate into the gravity domain (Fig. 12b). As will be shown in Section 5, overall the differences can be interpreted as improvements between the two Bedmap releases.

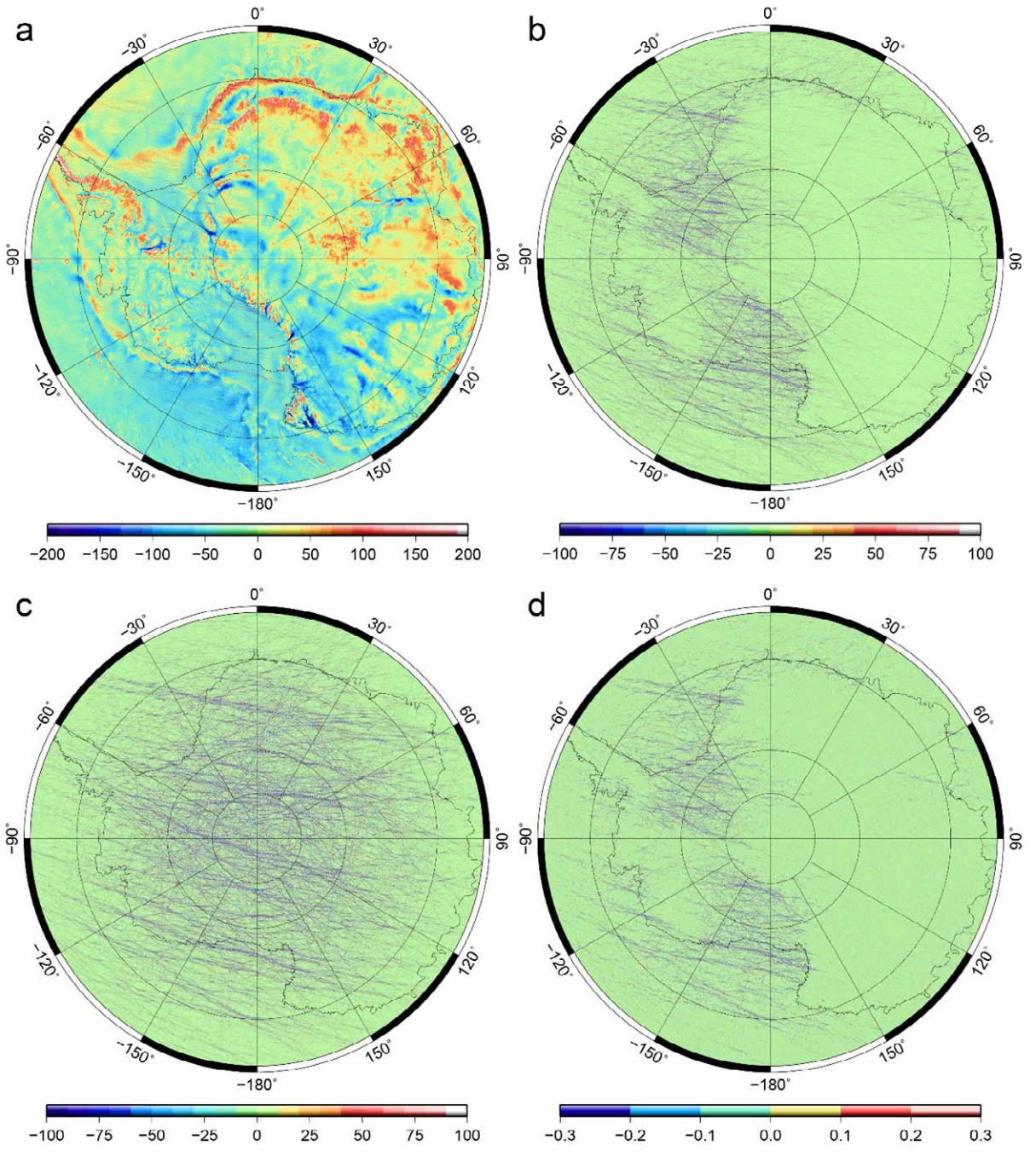

Fig. 13 Importance of including spectral band 2161-2190 in the gravity synthesis, exemplified with the SatGravRET2014_A geopotential model. Gravity disturbances at the topographic surface in band of harmonic degrees (a) 2 to 2160 (note the corrugations overlaying the field), (b) 2161 to 2190, (c) gravity disturbances evaluated at the GRS80 ellipsoid surface in the band 2161 to 2190, and (d) quasigeoid heights evaluated at the topographic surface in band 2161 to 2190. Units are in mGal (panels a-c) and in meters (panel d)

Importance of coefficients in band 2161 to 2190

Because the modelling technique applied for the computation of the Bedmap2 topographic potential is relatively new (cf. Claessens and Hirt 2013), and has not been investigated yet for gravity modelling over Antarctica, the relevance of the high-degree coefficients in spectral band of degrees 2161-2190 shall be emphasized. Fig. 13 (panel a) shows gravity disturbances of the SatGravRET2014 model deliberately truncated at degree 2160. High-frequency "corrugations" become visible, particularly in the lower-elevated Western Antarctica. Evaluation of gravity disturbances in harmonic band 2161 to 2190 (Fig. 13b) clearly shows the corrugations, however, with opposite sign. From Table 3, the RMS signal strength is ~17 mGal and maximum values exceed 100 mGal. Evaluation in harmonic band 2 to 2190 (that is, addition of gravity from panels 13a and 13b) removes the corrugations completely and gives the "corrugation-free" signals shown in Fig. 9c.

The signal strengths in spectral band 2161 to 2190 are even higher at the surface of the GRS80 reference ellipsoid (30 mGal RMS), Fig. 13c. Evaluation at the topographic surface reduces the effect (by virtue of gravity attenuation with height) over the elevated ice-masses of Eastern Antarctica only (Fig. 13b). For quasigeoid heights, the additional coefficients in band 2161 to 2190 reach 5 cm RMS signal strengths (or 40 cm amplitudes), Fig13d. This demonstrates the importance of taking spectral band 2161 to 2190 into account in any accurate evaluation of the SatGravRET2014 model to high degree.

By way of comparison, a very closely-related behaviour is known from EGM2008 (Pavlis et al. 2012) which features additional coefficients in band 2161-2190 too (also see Holmes et al. 2007 for details). These are equally important for precise computation of gravity field functionals over the Polar Regions as in case of SatGravRET2014.

4.2 Spectral domain

We compared the spectral energy of the SatGravRET2014 and SatGravETOPO1 models with selected models (EGM2008 and GOCE-TIM5) globally and locally over continental Antarctica, Fig. 14. We computed localized spectra of gravity disturbances from the four models, derived with power spectral density (PSD) functions and the 2D-discrete Fourier transform (2D-DFT) approach by Forsberg (1984b). We refer to Rexer and Hirt (2015) for full details on the computational procedure applied. The method is well suitable to compare the spectral energy of the models in a relative sense, also see Jekeli (2010).

Before applying the 2D-DFT the latitude-longitude gravity grids were transformed into polar-stereographic coordinates. The spectra refer to the gravity field signal (through gravity disturbances in $mGal^2$) over continental Antarctica only, which was achieved by setting ocean points (as identified through the land-mask in Fig. 2b) to zero. From Fig. 14a the gain in short-scale spectral energy in the band ranging from degree ~170 (~280) to ~2190 through gravity forward modelling in the two combined models is clearly visible in comparison to the satellite-only data from EGM2008 and GOCE-TIM5. Further to this, the comparison indicates that – relative to SatGravRET2014 – the SatGravETOPO1 model is somewhat underpowered in harmonic band ~250 to 2190, and this effect increases the higher the harmonic degree (Fig. 14a). This observation is thought to reflect the lack of sufficiently detailed (in the sense of short-scale) bedrock data over several areas in Bedmap1, also see Lythe et al. (2001) and Fretwell et al. (2013).

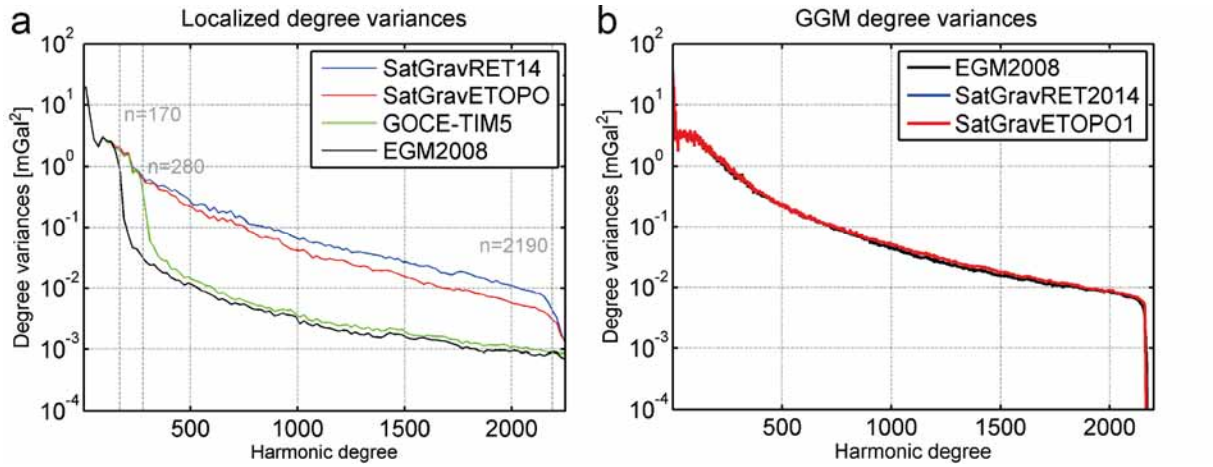

Fig.14. Spectral power of selected global models. Panel a: localized power spectra of gravity disturbances from EGM2008 (black), GOCE-TIM5 (green), SatGravRET2014 (blue) and SatGravETOPO1 (red) over continental Antarctica (spectra from 2D-DFT). Panel b: global power spectra of EGM2008 (black), SatGravRET2014 (blue) and SatGravETOPO1 (red, very similar with blue curve) (spectra from SHCs).

Fig. 14b shows dimensionless degree variance spectra of the two combined models and of EGM2008, all computed (globally) from the SHCs. The spectral behaviour of the combined models are very similar to EGM2008, all models have comparable energy throughout the spectrum, also at short scales (> degree 226) where the topographic masses are used as proxy to define the gravity field signals. This shows that the strengths of topography-modelled signals are commensurate with observation-based at short scales (Claessens and Hirt 2013). Note that all global spectra feature a "tail" in band 2161-2190, the effect of which has been discussed in detail in Fig. 13 (see also section 4.1). A further cross-comparison shows that the local power spectrum of the SatGravRET2014 model (Fig 14a) is well commensurate with those of EGM2008 and SatGravRET2014 globally (Fig. 14b).

5 Validation

The six airborne gravimetry data sets (Table 1) selected from the AntGG database were used for a comprehensive validation of the SatGravRET2014 model and several modelling variants, varying (i) the weighting schemes A,B,C, and (ii) the topographic data (Bedmap2 vs. Bedmap1) used. To benchmark the gain over satellite-only models, EGM2008 and GOCE-TIM5 were included in the comparisons. We compared gravity disturbances from all models and from the AntGG database at the topographic surface of Antarctica as represented by the Earth2014 surface layer. The descriptive statistics of the differences modelled minus observed gravity disturbance are reported in Table 5 (for sets #12 to #14) and in Table 6 (for sets #15 to #17). As further variants, the comparisons could be done at flight height, providing feedback on the downward-continuation process (cf. Holmes and Roman 2010, Smith et al. 2013). However, this is beyond the scope of the present paper.

From an initial inspection of the statistics (Tables 5 and 6), the mean values reach notable amplitudes of some 10s of mGal for data sets #12 to #15, while being at the 1mGal level for sets #16 and #17. The bias is found to be fairly independent of the model tested, but clearly dependent on the respective data set. For reasons described in Section 2.3 we interpret these mean values as bias in the airborne data. To reduce its impact on the evaluation of our gravity modelling, we use the standard deviation (STD) rather than the RMS as key performance indicator (akin a simple bias fit). This is justified because our focus is on benchmarking the medium and short-wavelength performance of the forward-modelling technique where offsets are not a concern.

Table 5. Descriptive statistics of comparisons of gravity disturbances from models EGM2008, GOCE-TIM5, SatGravRET2014_A,B,C and SatGravETOPO1_A,B,C against AntGG gravity (in the sense: model minus observation) over test areas 12,13 and 14. The last two columns report the improvement in STD (in percent) w.r.t EGM2008 and GOCE-TIM5.

Area	Model	Min	Max	Mean	RMS	STD	%EGM08	%TIM5
12	EGM08	-114.6	31.6	-41.1	44.5	17.2	-	-
	GOCE-TIM5	-121.5	38.2	-41.0	43.9	15.6	9.2	-
	SatGravRET2014_A	-102.8	18.5	-40.9	42.9	12.9	24.9	17.3
	SatGravRET2014_B	-103.4	19.3	-40.8	42.8	12.9	24.9	17.3
	SatGravRET2014_C	-104.2	17.9	-40.8	42.8	12.8	25.7	18.1
	SatGravETOPO1_A	-100.6	15.6	-41.0	43.2	13.8	20.2	12.1
	SatGravETOPO1_B	-103.0	14.7	-41.0	43.3	13.8	19.8	11.6
	SatGravETOPO1_C	-105.8	14.4	-41.0	43.2	13.7	20.5	12.4
13	EGM08	-97.4	53.7	-25.2	32.7	20.8	-	-
	GOCE-TIM5	-98.4	34.6	-25.9	32.2	19.1	8.2	-
	SatGravRET2014_A	-74.9	26.8	-25.1	28.1	12.7	39.1	33.7
	SatGravRET2014_B	-72.6	27.1	-25.0	28.1	12.8	38.7	33.3
	SatGravRET2014_C	-70.9	26.5	-25.0	28.3	13.2	36.8	31.2
	SatGravETOPO1_A	-89.6	41.8	-25.0	30.3	17.2	17.7	10.3
	SatGravETOPO1_B	-89.4	42.7	-25.0	30.3	17.2	17.5	10.1
	SatGravETOPO1_C	-92.0	44.0	-25.0	30.5	17.4	16.5	9.1
14	EGM08	-142.4	48.7	-32.8	38.2	19.5	-	-
	GOCE-TIM5	-159.5	74.2	-28.2	38.6	26.4	-34.9	-
	SatGravRET2014_A	-105.8	57.8	-33.5	37.9	17.7	9.4	32.8
	SatGravRET2014_B	-110.7	64.3	-33.2	38.1	18.7	4.5	29.2
	SatGravRET2014_C	-104.6	70.0	-31.8	37.5	19.9	-1.7	24.6
	SatGravETOPO1_A	-94.1	46.9	-34.6	40.2	20.4	-4.6	22.5
	SatGravETOPO1_B	-96.7	54.8	-33.8	40.2	21.7	-11.3	17.5
	SatGravETOPO1_C	-103.2	58.4	-31.7	39.5	23.6	-20.8	10.5

SatGravRET2014 vs. satellite-only data

The STD-values in Tables 5 and 6 consistently demonstrate over any of the six areas significant improvements of our SatGravRET2014 models over the satellite-only GOCE-TIM5 model. The reduction in STD varies between ~11 % (#15, reduction from ~17 to ~15 mGal STD) and ~60% (#16, reduction from ~20 to ~8 mGal). This shows that the Bedmap2 data carries significant information on short-scale gravity field constituents which has been successfully used in SatGravRET2014 for refinement of satellite gravimetry.

In comparison against EGM2008, the improvement rates are mostly higher (up to a very significant 75 % reduction in STD seen for data set #16) which reflects the use of GOCE satellite gravimetry to define the medium wavelength constituents of SatGravRET2014. The added-value of GOCE over EGM2008 is also seen in the direct comparisons in Tables 5 and 6.

Differences between four models and observations are shown in Fig. 15 for data set #17, exemplifying the increasingly improved agreement from EGM2008 (panel a) via GOCE-TIM5 (panel b) to the

SatGravRET2014 model (panel c). The remaining oscillations (amplitudes of about ±15 mGal) in Fig. 15c likely reflect the influence of unknown mass-density anomalies not represented by the RET2014 data set as well as uncertainties in the Bedmap2 data set. This indicates the limitations of the forward gravity modelling. In Fig. 15c the largest discrepancies (>50 mGal) between SatGravRET2014 and AntGG gravity are found in the "neighbourhood" of gaps in the surveys; these coincide with areas where Bedmap2 bedrock estimates are not based on observations either (Fig. 2 and Fretwell et al. 2013). Over these areas, large uncertainties of Bedmap2 bedrock information propagate into the gravity model as confirmed through comparisons with airborne gravimetry (Fig. 15c).

Table 6. Descriptive statistics of comparisons of gravity disturbances from models EGM2008, GOCE-TIM5, SatGravRET2014_A,B,C and SatGravETOPO1_A,B,C against AntGG gravity (in the sense model minus observation) over test areas 15,16 and 17. The last two columns report the improvement in STD (in percent) w.r.t EGM2008 and GOCE-TIM5.

Area	Model	Min	Max	Mean	RMS	STD	%EGM08	%TIM5
15	EGM08	-84.1	96.2	15.6	25.8	20.6	-	-
	GOCE-TIM5	-66.4	72.9	12.6	21.2	17.0	17.5	-
	SatGravRET2014_A	-62.0	71.7	12.9	19.7	14.9	27.9	12.6
	SatGravRET2014_B	-60.7	72.8	12.8	19.8	15.1	26.8	11.3
	SatGravRET2014_C	-61.7	76.1	12.9	19.7	14.9	27.4	12.1
	SatGravETOPO1_A	-58.8	75.9	12.9	20.7	16.2	21.3	4.6
	SatGravETOPO1_B	-58.5	76.7	13.0	21.1	16.6	19.4	2.4
	SatGravETOPO1_C	-59.9	74.3	13.2	21.0	16.4	20.4	3.5
16	EGM08	-70.0	95.0	5.8	35.1	34.6	-	-
	GOCE-TIM5	-56.3	54.7	-0.7	20.3	20.3	41.3	-
	SatGravRET2014_A	-23.3	28.9	1.5	8.7	8.6	75.2	57.8
	SatGravRET2014_B	-21.9	29.5	1.6	8.5	8.3	76.0	59.1
	SatGravRET2014_C	-19.5	31.0	1.7	8.1	7.9	77.1	61.0
	SatGravETOPO1_A	-68.6	70.1	-0.4	22.1	22.1	36.2	-8.6
	SatGravETOPO1_B	-67.4	67.9	-0.4	21.6	21.6	37.6	-6.3
	SatGravETOPO1_C	-64.7	63.9	-0.5	20.7	20.7	40.2	-1.9
17	EGM08	-129.4	78.3	0.4	18.0	18.0	-	-
	GOCE-TIM5	-128.2	80.3	0.0	16.0	16.0	10.8	-
	SatGravRET2014_A	-62.3	193.8	-1.5	13.4	13.3	26.0	17.0
	SatGravRET2014_B	-62.7	193.3	-1.5	13.3	13.3	26.3	17.4
	SatGravRET2014_C	-61.1	190.3	-1.4	13.3	13.2	26.7	17.8
	SatGravETOPO1_A	-89.0	195.2	-1.1	18.6	18.6	-3.1	-15.7
	SatGravETOPO1_B	-89.0	195.3	-1.1	18.5	18.5	-2.7	-15.2
	SatGravETOPO1_C	-87.8	192.8	-1.0	18.1	18.1	-0.3	-12.5

Performance over the South Pole region

Of particular value is the Transantarctic Mountains – South Pole Transect (data set #14) showing the influence of the polar gap problem on the GOCE model performance. Because of GOCE's orbit inclination (83.3°) the gravity field over the South Pole region could not be directly observed. As a result some of the near-zonal SHCs of the GOCE-only model TIM5 are weakly determined, the effect of which is manifesting in a larger disagreement with the AntGG data than EGM2008 (19.5 vs. 26.4

mGal in terms of STD, or deterioration by ~35 %, cf. Table 5). This effect is also present in the combined models which offer only little improvement over the GRACE-observations of EGM2008 around the South Pole. Particularly the inter-comparison between the weighting schemes C, B, and A reveals the less GOCE information is used in the combination (and, thus, the longer the associated wavelengths where Bedmap2 information defines the SatGravRET2014 models), the better the fit with the airborne gravimetry data. This is seen from the improvement rates raising from -1.7% (scheme C) to ~9.4% (scheme A). As such, the comparisons demonstrate that the polar gap problem cannot be solved but at least mitigated to some extent by choosing an "appropriate" weighting scheme.

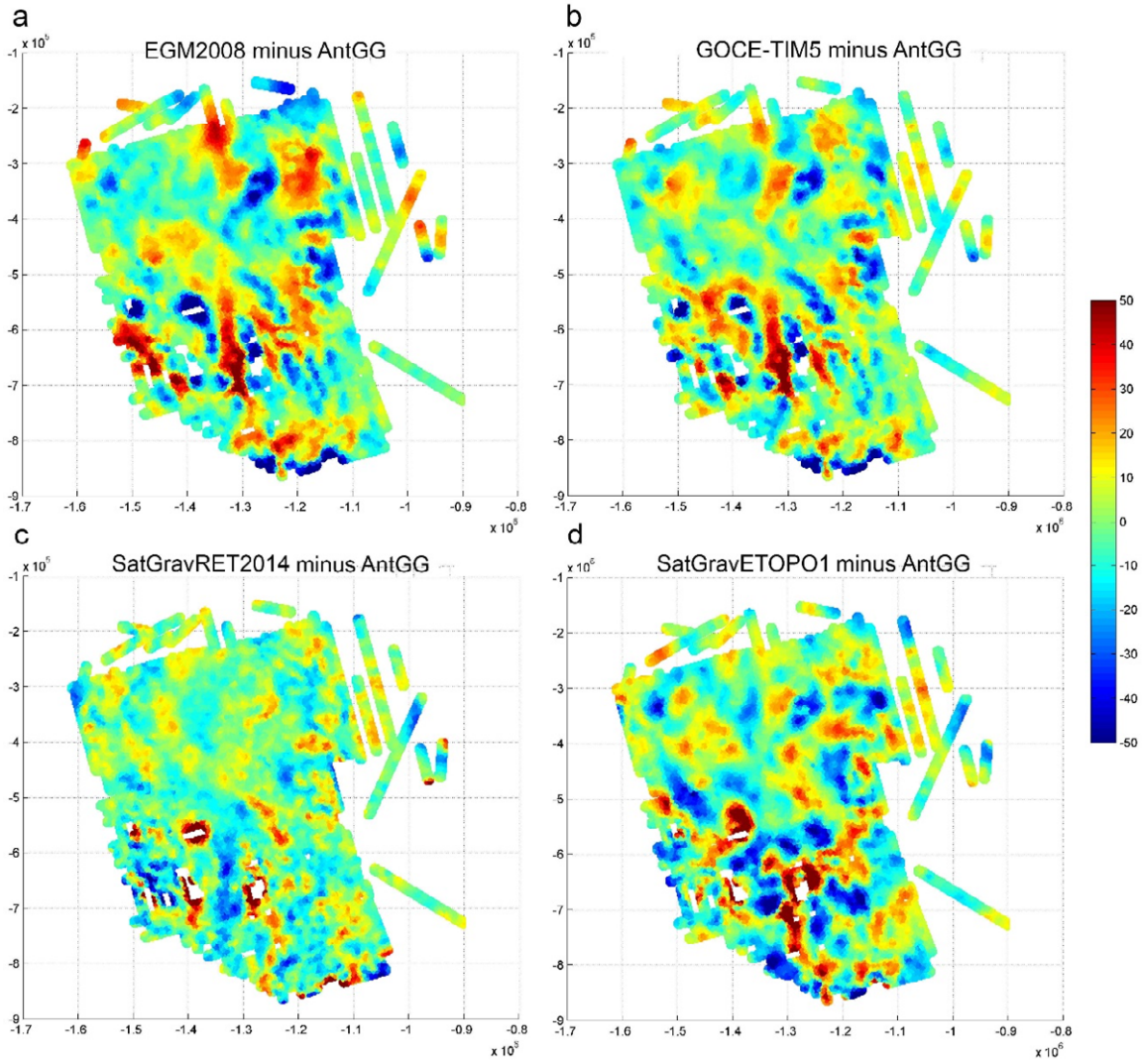

Fig. 15 Residuals from comparison of (a) EGM2008 (b) GOCE-TIM5, (c) SatGravRET2014_A, and (d) SatGravETOPO1_A gravity disturbances against AntGG airborne gravimetry data set #17. Units in mGals, projection is polar-stereographic, coordinates give distance to the South Pole (in meters)

Preferred weighting scheme

Apart from the Transantarctic Mountains – South Pole Transect (data set #14) the other five data sets show only marginal differences in performance between the SatGravRET2014 modelling variants A, B and C (compare STD values in Tables 5 and 6 which differ only by few 0.1 mGal). Weighting scheme A produces the best fit over area #13 and #14, while scheme C is best over areas #12, #16 and #17 (over area #15, both schemes equally produce the lowest STD values). Because the differences in STD are very small over most areas apart from #14, the choice of the scheme does have fairly little impact on the SatGravRET2014 model quality *outside the polar gap.* Notwithstanding scheme A is clearly superior

to B and C *inside the polar gap region*. Therefore weighting scheme A and the associated solution SatGravRET2014_A = SatGravRET2014 is our preferred solution from the ones tested in our study.

Bedmap2 vs. Bedmap1

The comparisons in Tables 5 and 6 provide a very clear picture on the value of Bedmap2 for high-resolution gravity modelling over Antarctica. All data sets consistently show lower STD values and higher improvement rates for SatGravRET2014 than for the Bedmap1-based SatGravETOPO1 model, both in comparison to EGM2008 and to GOCE-TIM5 and for all comparisons across the three weighting schemes, too. The differences between the Bedmap2 and Bedmap1 performance are very pronounced over some regions, e.g. data set #13, where Bedmap2-associated improvement rates are ~30-40 % while only 10-18 % for Bedmap1. Over regions #16 and #17 compared to GOCE-only, the use of Bedmap1 topographic gravity at spatial scales of 80 to 10 km even deteriorates the agreement with AntGG gravity (negative rates ranging between ~-2% to ~ -16%), while Bedmap2 improves by 17% to 60%. A detailed impression of the Bedmap2 vs. Bedmap1 performance is given in Fig. 15 for data set #17, where the Bedmap1-dependent SatGravETOPO1 model in many places produces discrepancies at the 30mGal-level (Fig. 15d). These features are not visible for the Bedmap2-dependent SatGravRET2014 model (Fig. 15c).

All these comparisons provide strong evidence for the improvements in Bedmap2 topography, ice and bedrock data over the previous Bedmap1 release, while showing the limitations of the Bedmap1 release for gravity modelling. These were encountered by Schwabe et al. (2012), too, who found Bedmap1 to be of limited value for smoothing of observed gravity. Because the topographic surface was reasonably well known in Bedmap1 already (Lythe et al. 2001), our comparisons provide evidence that the knowledge of the bedrock geometry (and hence density contrast rock vs. ice) has considerably more impact on the quality of the derived gravity field than the surface topography over Antarctica.

6 Discussion and conclusions

This study has presented the new SatGravRET2014 global gravitational model constructed as a combination of satellite gravity (GRACE and GOCE missions) with topography-implied gravity from the Bedmap2 data compilation. Our model resolves the gravity field over continental Antarctica for the first time to ~10 km spatial scales, or to harmonic degree 2190. Comprehensive validation based on AntGG airborne gravimetry has shown that the short-scale Bedmap2-based gravity modelling improves over satellite-only models by 8 to 75%. As such, the application of the described modelling techniques along with the Bedmap2 product is proven to be an alternative to the RTM fill-in techniques by Pavlis et al. (2007) and, thus, is an effective way for refining the Antarctic gravity field to short spatial scales. The SatGravRET2014 model may be of some utility for determining biases in airborne gravimetric surveys, as was indicated in this paper. Also other applications which require spectrally complete gravity information could benefit from the SatGravRET2014 model.

As a main characteristic of the modelling technique used, information on mass-density anomalies other than represented by the Bedmap2 product has not been used to define the short-scale gravity field constituents (at scales of 80 to 10 km) over Antarctica. However, this shortcoming can be reduced in the future over parts of Antarctica through combination with observed gravity, notably the AntGG gravity database (Scheinert et al. 2015). As further possible extensions of the presented work, modelling of the ice masses as mass-layers (e.g., Tenzer et al. 2010, 2015) rather than via RET-compression, as well as extending the modelling resolution to scales less than 10 km, e.g., with the RTM augmentation technique (Forsberg 1984a, Hirt et al. 2014) are expected to yield further improvements.

It is clear that over most areas outside continental Antarctica the SatGravRET2014 model cannot be "competitive" with other degree-2190 GGMs (EGM2008 and EIGEN-6C4) both of which are based on observed gravity over large parts of Earth's surface down to 10 km scales. This is because observations capture the gravity field generally in a better way than topography-based forward modelling is able to approximate it (for a detailed investigation of the performance of topography-based gravity field modelling at spatial scales not resolved by GOCE see e.g., Hirt et al. 2012).

While combinations of SatGravRET2014 with AntGG will further improve the modelling of the Antarctic gravity field, our model will be of particular value as a proxy of the gravity field over all regions devoid of airborne gravity but covered by Bedmap2 ice-thickness data. Over those regions, ice thickness measurements are of sufficient quality to improve satellite-only gravity information through gravity forward modelling, as shown in this study. The situation is very different over those parts of Antarctica devoid of airborne gravity and radar ice thickness measurements (e.g., partially inside the GOCE polar gap) where neither approach is capable of delivering detailed gravity field knowledge.

A focus was on comparisons between Bedmap1 and Bedmap2 for detailed mass modelling over Antarctica. Using airborne gravimetry as a validation tool, our comparisons unambiguously demonstrate the improvements in Bedmap2 bedrock knowledge over Bedmap1 at spatial scales ~80 to 10 km. Our validation results complement those by Hirt (2014) who used GOCE satellite gravimetry as a means to demonstrate the Bedmap2-added value at scales of ~400 to 80 km. Holistically, these results underline the usefulness of the Bedmap2 product for detailed gravity modelling over Antarctica, as in the SatGravRET2014 model, or as future extension of the GGMplus gravity maps (Hirt et al. 2013) towards the Polar Regions.

Conversely, the lack of detailed bedrock data over many areas in Bedmap1 has implications for the short-scale quality of current topographic gravity models derived from ETOPO1 (and thus, from Bedmap1). Examples are the World Gravity Map (WGM, Balmino et al. 2012, Bonvalot et al. 2012) and the topographic potential models currently available via IAG's ICGEM (e.g., the RWI model by Grombein et al. 2014 and dV_ELL_RET2012 by Claessens and Hirt 2013), all using Bedmap1 information. These models and maps should be used with some caution over continental Antarctica unless updated with Bedmap2.

Acknowledgements

We thank three anonymous reviewers for their comments on this manuscript. This study received support from the Australian Research Council (ARC, grant DP120102441) and Curtin University's Office of Research and Development. Further, it was created with the support of the Technische Universität München - Institute for Advanced Study, funded by the German Excellence Initiative. Christian Hirt is the recipient of an ARC Discovery Outstanding Researcher Award and of a Hans-Fischer Fellowship by IAS. Parts of the computations were carried out with resources provided by the Leibniz Rechenzentrum München. We thank Jan-Martin Brockmann for providing GOCE data sets and Thomas Fecher for providing routines for solving of normal equations. The topographic potential model dV_ELL_RET2014 and combined SatGravRET2014 model will be delivered to IAG's ICGEM service (http://icgem.gfz-potsdam.de/ICGEM/). Our models are also available via ddfe.curtin.edu.au/models/Antarctica. The topographic input data sets used in this study can be downloaded from ddfe.curtin.edu.au/models/Earth2014.

Appendix A

The fully normalised sinusoidal Legendre weight functions $\bar{K}_{nm}^{2i,2j}$ in Eq. (25) can be computed via various recursive schemes (Claessens 2005)

$$\bar{K}_{nm}^{2i,2j} = \sum_{k=-1}^{1} \bar{K}_{nm}^{2i-2k,2j-2} \bar{K}_{n+2i-2k,m}^{2k,2} \tag{A1}$$

$$\bar{K}_{nm}^{2i,2j} = \sum_{k=-1}^{1} \bar{K}_{nm}^{2k,2} \bar{K}_{n+2k,m}^{2i-2k,2j-2} \tag{A2}$$

$$\bar{K}_{nm}^{2i,2j} = \sum_{k=-1}^{1} \bar{K}_{nm}^{2i+2k,2j-2} \bar{K}_{n+2i,m}^{2k,2} \tag{A3}$$

where (A3) follows from (A1) and the relation

$$\bar{K}_{nm}^{2i,2j} = \bar{K}_{n+2i,m}^{-2i,2j} \tag{A4}$$

Equations (A1) to (A3) can all be used to compute the function $\bar{K}_{nm}^{2i,2j}$ for any pair of *i* and *j* from the initial values

$$\bar{K}_{nm}^{-2,2} = -\sqrt{\frac{(n^2-m^2)[(n+1)^2-m^2]}{(2n-3)(2n-1)^2(2n+1)}} \tag{A5}$$

$$\bar{K}_{nm}^{0,2} = \frac{2(n^2+m^2+n-1)}{(2n-1)(2n+3)} \tag{A6}$$

$$\bar{K}_{nm}^{2,2} = -\sqrt{\frac{[(n+1)^2-m^2][(n+2)^2-m^2]}{(2n+1)(2n+3)^2(2n+5)}} \tag{A7}$$

References

Amante C, Eakins BW (2009) ETOPO1 1 Arc-Minute Global Relief Model: Procedures, Data Sources and Analysis. NOAA Technical Memorandum NESDIS NGDC-24, 19 pp, March 2009.

Balmino G, Vales N, Bonvalot S, Briais A (2012) Spherical harmonic modelling to ultra-high degree of Bouguer and isostatic anomalies J Geod 86(7):499-520. doi: 10.1007/s00190-011-0533-4

Bamber JL, Griggs JA, Hurkmans RT, et al. (2013) A new bed elevation data set for Greenland. The Cryosphere 7: 499-510.

Becker JJ, Sandwell DT, Smith WHF, et al. (2009) Global Bathymetry and Elevation Data at 30 Arc Seconds Resolution: SRTM30_PLUS. Mar Geod 32(4):355-371.

Bell RE, Childers VA, Arko RA, Blankenship DD, Brozena JM (1999) Airborne gravity and precise positioning for geologic applications. J. Geophys. Res., 104(B7), 15,281–292. doi:10.1029/ 1999JB900122

Bonvalot S, Balmino G, Briais A, Kuhn M, Peyrefitte A, Vales N (2012) World Gravity Map, 1:50,000,000 map, Eds.: BGI-CGMW-CNES-IRD, Paris.

Bucha B, Janák J (2014) A MATLAB-based graphical user interface program for computing functionals of the geopotential up to ultra-high degrees and orders: Efficient computation at irregular surfaces. Comp Geosc 66:219-227. 10.1016/j.cageo.2014.02.005

Brockmann JM, Zehentner N, Höck E, Pail R, Loth I, Mayer-Gürr T, Schuh W-D (2014) EGM_TIM_RL05: An independent geoid with centimeter accuracy purely based on the GOCE mission. Geophys Res Lett 41(22): 8089–8099. doi: 10.1002/2014GL061904

Claessens SJ (2005) New relations among associated Legendre functions and spherical harmonics. J Geod 79(6-7):398-406. doi: 10.1007/s00190-005-0483-9

Claessens SJ (2006) Solutions to Ellipsoidal Boundary Value Problems for Gravity Field Modelling. PhD thesis, Curtin University of Technology, Perth, Western Australia

Claessens SJ, Hirt C (2013) Ellipsoidal topographic potential – new solutions for spectral forward gravity modelling of topography with respect to a reference ellipsoid, J Geophys Res – Solid Earth 118(11):5991-6002. doi: 10.1002/2013JB010457

Davis M (2001) Subglacial Morphology and Structural Geology in the Southern Transantarctic Mountains from Airborne Geophysics, M.S. Thesis, University of Texas, 133pp

Diehl T, Holt J, Blankenship D, Young D, Jordan T, Ferraccioli F (2008) First airborne gravity results over the Thwaites Glacier catchment, West Antarctica. Geochem. Geophys. Geosyst. 9(4), Q04011. doi:10.1029/ 2007GC001878

Fecher T, Pail R, Gruber T (2015) Global gravity field modeling based on GOCE and complementary gravity data. Intern. J Appl. Earth Obs Geoinf 35:120–127. doi:10.1016/j.jag.2013.10.005

Flury J, Rummel R (2005) Future satellite gravimetry for geodesy. Earth Moon Planets 94: 13–29. doi: 10.1007/s11038-005-3756-7

Forsberg R (1984a) Local Covariance Functions and Density Distribution. OSU Report 356, Department of Geodetic Science and Surveying, Ohio State University, Columbus.

Forsberg R (1984b) A study of terrain reductions, density anomalies and geophysical inversion methods in gravity field modelling. OSU Report 355. Department of Geodetic Science and Surveying, Ohio State University, Columbus.

Forsberg R, Olesen AV, Yildiz H, Tscherning CC (2011) Polar Gravity Fields From GOCE And Airborne Gravity, Proc of 4th International GOCE User Workshop, Munich, Germany, ESA SP-696, July 2011.

Förste C, Bruinsma SL, Abrikosov O, Lemoine J-M, Schaller T, Götze H-J, Ebbing J, Marty JC, Flechtner F, Balmino G, Biancale R (2014) EIGEN-6C4 The latest combined global gravity field model including GOCE data up to degree and order 2190 of GFZ Potsdam and GRGS Toulouse; presented at the 5th GOCE User Workshop, Paris, 25-28 November 2014

Fretwell P, Pritchard HD, Vaughan DG, Bamber JL, et al. (2013) Bedmap2: improved ice bed, surface and thickness data sets for Antarctica. The Cryosphere 7: 375-393.

Grombein, T, Luo X, Seitz K, Heck B (2014) A wavelet-based assessment of topographic isostatic reductions for GOCE gravity gradients. Surv Geophys 35(4):959-982. doi:10.1007/s10712-014-9283-1

Hirt C (2012) Efficient and accurate high-degree spherical harmonic synthesis of gravity field functionals at the Earth's surface using the gradient approach. J Geod 86(9):729-744, doi:10.1007/s00190-012-0550-y

Hirt C., Claessens S.J., Kuhn M., Featherstone W.E. (2012) Indirect evaluation of Mars Gravity Model 2011 using a replication experiment on Earth. Studia Geophysica and Geodetica, 56 (2012): 957-975. doi: 10.1007/s11200-011-0468-5

Hirt C, Claessens SJ, Fecher T, Kuhn M, Pail R, Rexer M (2013) New ultra-high resolution picture of Earth's gravity field. Geophys Res Lett 40(16): 4279–4283. doi:10.1002/grl.50838

Hirt C (2014) GOCE's view below the ice of Antarctica: Satellite gravimetry confirms improvements in Bedmap2 bedrock knowledge. Geophys Res Lett 41(14):5021-5028. doi: 10.1002/2014GL060636

Hirt C, Kuhn M, Claessens SJ, Pail R, Seitz K, Gruber T (2014) Study of the Earth's short-scale gravity field using the ERTM2160 gravity model. Comp Geosci 73:71-80. doi: 10.1016/j.cageo.2014.09.00

Hirt C, Kuhn M (2014) Band-limited topographic mass distribution generates a full-spectrum gravity field – gravity forward modelling in the spectral and spatial domain revisited. J. Geophys Res – Solid Earth, 119(4): 3646–3661. doi: 10.1002/2013JB010900

Hirt, C, Rexer M (2015) Earth2014: 1 arc-min shape, topography, bedrock and ice-sheet models - available as gridded data and degree-10,800 spherical harmonics. Int J Appl Earth Obs Geoinf 39, 103-112. doi:10.1016/j.jag.2015.03.001.

Hirt C, Rexer M, Claessens SJ (2015) Topographic evaluation of fifth-generation GOCE gravity field models - globally and regionally, Newton's Bulletin 5, Special issue on validation of GOCE gravity fields, 163-186.

Holmes SA, Featherstone WE (2002) A unified approach to the Clenshaw summation and the recursive computation of very high degree and order normalized associated Legendre functions. J Geod 76(5):279-299. doi: 10.1007/s00190-002-0216-2

Holmes SA (2003) High degree spherical harmonic synthesis for simulated earth gravity modelling. PhD Thesis, Department of Spatial Sciences, Curtin University of Technology, Perth, Western Australia.

Holmes SA, Pavlis NK (2007) Some Aspects of Harmonic Analysis of Data Gridded on the Ellipsoid. Proceedings of the 1st International Symposium of the International Gravity Field Service (IGFS), Istanbul, pp 151-156.

Holmes SA, Roman D (2010), The Application of High-Degree Gravitational Models to Processing Airborne Gravity Collected under the NGS GRAV-D Project, Paper presented at FIG Congress 2010, Facing the Challenges – Building the Capacity, Sydney, Australia, 11-16 April 2010

Holt J, Richter T, Kempf S, Morse D, Blankenship D (2006) Airborne gravity over Lake Vostok and adjacent highlands of East Antarctica. Geochem. Geophys. Geosyst., 7(11), Q11012. doi:10.1029/ 2005GC001177

Jarvis, A., Reuter, H.I., Nelson, A., Guevara, E., 2008. Hole-filled SRTM for the globe v4.1, Available from the CGIAR-SXI SRTM 90m database at: http://srtm.csi.cgiar.org.

Jekeli, C (1988) The exact transformation between ellipsoidal and spherical expansions. Manuscripta Geodaetica 13:106-113

Jekeli C (2010) Correlation Modeling of the Gravity Field in Classical Geodesy, In: W. Freeden, M.Z. Nashed, T. Sonar (Eds.), Handbook of Geomathematics 833-866. doi:10.1007/978-3-642-01546-5_28

Luyendyk, B., Wilson D, Siddoway C (2003) Eastern margin of the Ross Sea Rift in western Marie Byrd Land, Antarctica: Crustal structure and tectonic development, Geochem. Geophys. Geosyst., 4(10), 1090. doi:10.1029/2002GC000462.

Lythe, MB, Vaughan DG, and the Bedmap Consortium (2001) BEDMAP: A new ice thickness and subglacial topography model of Antarctica. J Geoph Res. 106(B6): 11335-11351. doi:10.1029/2000JB900449

Mayer-Gürr, T, Kurtenbach E, Eicker A (2010) ITG-Grace2010: the new GRACE gravity field release computed in Bonn, paper presented at European Geosciences Union General Assembly 2010, Geophys. Res. Abstr., 12, EGU2010-2446, Vienna, Austria.

Mayer-Gürr T, Rieser D, Höck E, Brockmann JM, Schuh W-D, Krasbutter I, Kusche J, Maier A, Krauss S, Hausleitner W, Baur O, Jäggi A, Meyer U, Prange L, Pail R, Fecher T, Gruber T (2012) The new combined satellite only model GOCO03s. Abstract at GGHS2012, Venice (Poster).

McKenzie D, Yi W, Rummel R (2015) Estimates of Te for Continental Regions using GOCE gravity. Earth and Planetary Science Letters 399:116-127. doi:10.1016/j.epsl.2014.05.003.

Morgan PJ, Featherstone WE (2009) Evaluating EGM2008 over East Antarctica. In: Newton's Bulletin 4: 317-331.

O'Donnell JP, Nyblade AA (2014) Antarctica's hypsometry and crustal thickness: Implications for the origin of anomalous topography in Antarctica. Earth Plan Sci Lett 388:143-155. doi: 10.1016/j.epsl.2013.11.051

Pail R, Bruinsma S, Migliaccio F, Förste C, Goiginger H, Schuh W-D, Höck E, Reguzzoni M, Brockmann JM, Abrikosov O, Veicherts M, Fecher T, Mayrhofer R, Krasbutter I, Sansò F, Tscherning CC (2011) First GOCE gravity field models derived by three different approaches. J Geod 85(11): 819-843. doi:10.1007/s00190-011-0467-x

Pavlis NK, Factor JK, Holmes SA (2007) Terrain-related gravimetric quantities computed for the next EGM. Proceedings of the 1st International Symposium of the International Gravity Field Service (IGFS), Istanbul, pp 318-323.

Pavlis NK, Holmes SA, Kenyon SC, Factor JK (2012) The development and evaluation of the Earth Gravitational Model 2008 (EGM2008), Journal of Geophysical Research 117(B4): B04406.

Rapp RH (1997) Use of potential coefficient models for geoid undulation determinations using a spherical harmonic representation of the height anomaly/geoid undulation difference. J Geod 71(5):282-289.

Rexer, M, Hirt C (2015) Spectral analysis of the Earth's topographic potential via 2D-DFT - a new data-based degree variance model to degree 90,000. J Geod 89(9):887-909, doi:10.1007/s00190-015-0822-4

Rummel R, Rapp RH, Sünkel H, Tscherning CC (1988) Comparisons of global topographic/isostatic models to the Earth's observed gravity field, Report No 388, Dep. Geodetic Sci. Surv., Ohio State University, Columbus, Ohio.

Rummel R, Horwath M, Yi W, Albertella A, Bosch W, Haagmans R (2011) GOCE, satellite gravimetry and antarctic mass transports. Surv Geoph 32(4-5):643-657. doi:10.1007/s10712-011-9115-5

Rummel R (2013) Height unification using GOCE. J Geod Sci 2(4):355–362, doi: 10.2478/v10156-011-0047-2

Scheinert M, Müller J, Dietrich R, Damaske D, Damm V (2008) Regional geoid determination in Antarctica utilizing airborne gravity and topography data. J Geod 82(7):403-414. doi:10.1007/s00190-007-0189-2

Scheinert M (2012) Progress and prospects of the Antarctic Geoid Project (Commission Project 2.4), in Geodesy for Planet Earth, IAG Conf. Series, vol. 136, pp. 451–456, Springer, Berlin Heidelberg.

Scheinert, M, Ferraccioli F, Schwabe J, Bell R, Studinger M, Damaske D, Jokat W, Aleshkova N, Jordan T, Leichenkov G, Blankenship DD, Damiani TM, Young D (2015) New Antarctic Gravity Anomaly Grid for Enhanced Geodetic and Geophysical Studies in Antarctica, Geophys Res Lett, post-revision.

Schwabe, J, Scheinert M, Dietrich R, Ferracccioli F, Jordan T (2012) Regional geoid improvement over the Antarctic Peninsula Utilizing Airborne Gravity Data, in Geodesy for Planet Earth, IAG Conf. Series, vol. 136, pp. 457–464, Springer, Berlin Heidelberg.

Schwabe J, Ewert H, Scheinert M, Dietrich R (2014) Regional geoid modelling in the area of subglacial Lake Vostok, Antarctica. J Geodyn 75:9-21. doi:10.1016/j.jog.2013.12.002

Schwabe, J, Scheinert M (2014) Regional geoid of the Weddell Sea, Antarctica, from heterogeneous ground-based gravity data. J Geod 88(9):821-838. doi:10.1007/s00190-014-0724-x

Shepherd A, Ivins ER, Geruo A, et al. (2012) A reconciled estimate of ice sheet mass balance. Science 338:1183–1189, doi:10.1126/science.1228102

Smith DA, Holmes SA, Li X, Guillaume Y, Wang YM, Bürki B, Roman DR, Damiani TM (2013) Confirming regional 1 cm differential geoid accuracy from airborne gravimetry: the Geoid Slope Validation Survey of 2011. J Geod 87(10-12):885-907. doi:10.1007/s00190-013-0653-0

Sneeuw N, van Gelderen M (1997) The polar gap. In: Geodetic Boundary Value Problems in view of the One Centimeter Geoid (ed. Sanso F, Rummel R), Lecture Notes in Earth Sciences, 65: 559-568, Springer Berlin Heidelberg. doi: 10.1007/BFb0011717

Studinger, M, Bell R, Finn C, Blankenship D (2002) Mesozoic and Cenozoic extensional tectonics of the West Antarctic Rift System from high-resolution airborne geophysical mapping. Roy. Soc. of New Zealand Bull. 35, 563–569.

Studinger, M et al. (2003a) Ice cover, landscape setting, and geological framework of Lake Vostok, East Antarctica, Earth Planet. Sci. Lett., 205(3-4), 195–210, doi: 10.1016/S0012-821X(02)01041-5.

Studinger, M, Karner G, Bell R, Levin V, Raymond C, Tikku A (2003b) Geophysical models for the tectonic framework of the Lake Vostok region, East Antarctica. Earth Planet. Sci. Lett., 216(4), 663–677. doi: 10.1016/S0012-821X(03)00548-X

Studinger M, Bell RE, Roger Buck W, Karner GD, Blankenship DD (2004) Sub-ice geology inland of the Transantarctic Mountains in light of new aerogeophysical data. Earth Plan Sci Lett 220(3-4):391-408. doi:10.1016/S0012-821X(04)00066-4

Studinger M, Bell RE, Fitzgerald PG, Buck WR (2006) Crustal architecture of the Transantarctic Mountains between the Scott and Reedy Glacier region and South Pole from aerogeophysical data. Earth Plan. Sci. Lett., 250(1–2), 182 – 199. doi: 10.1016/j.epsl.2006.07.035

Tenzer, R, Abdalla A, Vajda P, Hamayun (2010) The spherical harmonic representation of the gravitational field quantities generated by the ice density contrast. Contrib Geophys Geod 40(3):207-223, doi:10.2478/v10126-010-0009-1

Tenzer R, Chen W, Tsoulis D, Bagherbandi M, Sjöberg LE, Novák P, Jin S (2015) Analysis of the Refined CRUST1.0 Crustal Model and its Gravity Field. Surv Geophys. 36:139–165, doi:10.1007/s10712-014-9299-6

Torge W, Müller J (2012) Geodesy, 4th Edition, de Gruyter, Berlin, New York.

van der Meijde M, Pail R, Bingham R, Floberghagen R (2013) GOCE data, models, and applications: A review, Int. J. Appl. Earth Obs. Geoinf. 35:4-15. doi:10.1016/j.jag.2013.10.001.

von Frese RRB, Potts LV, Wells SB, et al. (2009) GRACE gravity evidence for an impact basin in Wilkes Land, Antarctica, Geochem Geophys, Geosys 10(2):1-14. doi:10.1029/2008GC002149

Wessel P, Smith WHF, Scharroo R, Luis JF, Wobbe F (2013) Generic Mapping Tools: Improved version released, EOS Trans. AGU, 94, 409-410.